High-throughput Identification of Novel Heat Tolerance Genes via Genome-wide Pooled Mutant Screens in the Model Green Alga *Chlamydomonas reinhardtii*

Erin M. Mattoon[1,2], William McHargue[1,2], Catherine E. Bailey[1], Ningning Zhang[1], Chen Chen[3], James Eckhardt[1,6], Chris G. Daum[4], Matt Zane[4], Christa Pennacchio[4], Jeremy Schmutz[4], Ronan C. O'Malley[4&5], Jianlin Cheng[3], Ru Zhang[1,*]

*Corresponding author: Ru Zhang (rzhang@danforthcenter.org)

[1]Donald Danforth Plant Science Center, St. Louis, Missouri 63132, USA;

[2]Plant and Microbial Biosciences Program, Division of Biology and Biomedical Sciences, Washington University in Saint Louis, St. Louis, Missouri 63130, USA;

[3]Department of Electrical Engineering and Computer Science, University of Missouri, Columbia, Missouri 65211, USA;

[4]U.S. Department of Energy, Joint Genome Institute, Lawrence Berkeley National Laboratory, Berkeley, CA, USA;

[5]Environmental Genomics and Systems Biology, Lawrence Berkeley National Laboratory, Berkeley, CA, USA;

[6]Current address: University of California Riverside, Riverside, California, 92521, USA.

Abstract

High temperatures adversely affect crop and algal yields. Photosynthetic cells show varying physiological responses to different heat intensities. The specificity of genes required for thermotolerance at different temperatures in photosynthetic cells remains elusive. Additionally, organic carbon sources are present in nature for both plants and algae, but it is unclear how environmental availability of carbon sources interface with

heat responses. We utilized the insertional mutant library of the unicellular, eukaryotic green alga *Chlamydomonas reinhardtii* (CLiP) to perform genome-wide, quantitative, pooled screens under moderate (35°C) or acute (40°C) high temperatures with or without organic carbon. We screened for heat sensitive mutants based on growth rate quantification and identified putative heat tolerance genes (HTGs). By triangulating HTGs with heat-induced transcripts/proteins in wildtype cultures and MapMan functional annotation data, we present a high-confidence list of 933 *Chlamydomonas* genes with putative roles in heat tolerance. These include genes with known roles in thermotolerance and those with little or no functional annotation, suggesting novel players in thermotolerance. About 50% of these high-confidence HTGs in Chlamydomonas have orthologs in green lineage model organisms, including crop species. *Arabidopsis thaliana* mutants deficient in the ortholog of a *Chlamydomonas* HTG were also heat sensitive. This work expands our knowledge of heat responses in photosynthetic cells and provides engineering targets to improve thermotolerance in algae and crops.

Keywords: heat responses, heat tolerance genes, *Chlamydomonas reinhardtii*, CLiP mutant library, pooled screens, DNA barcodes

Introduction

Global warming increases the frequency of damaging high temperatures, which jeopardizes plant growth and reduces food/biofuel production (Janni *et al.* 2020). Nine of the ten hottest years on record have occurred between 2010-2021 (NASA, Goddard Institute for Space Studies). Global warming is predicted to reach 1.5°C above pre-industrial levels between 2030-2052 at the current warming rate (Intergovernmental Panel on Climate Change, IPCC, 2018) (Jagadish, Pal, Sukumaran, Parani & Siddique 2020). It is estimated that every degree Celsius increase in mean global temperature reduces global yields of wheat, rice, maize and soybean by 6%, 3.2%, 7.4% and 3.1%, respectively (Zhao *et al.* 2017). A recent model based on weather information and six major US crops from 1981-2017 identified high temperature as the primary climatic driver for yield reduction in crops (Ortiz-Bobea, Wang, Carrillo & Ault 2019). To engineer heat tolerant crops for the increasing human population, it is essential to understand how plants respond to high temperatures and which genes are required for thermotolerance.

55

56 High temperatures affect many cellular processes in plants(Mittler, Finka & Goloubinoff
57 2012; Schroda, Hemme & Mühlhaus 2015; Janni *et al.* 2020). They increase membrane
58 fluidity (Martinière *et al.* 2011), ion channel activities, and intracellular calcium
59 concentrations (Saidi *et al.* 2009; Mittler *et al.* 2012), reduce photosynthesis in
60 chloroplasts (Zhang & Sharkey 2009; Anderson *et al.* 2021; Zhang *et al.* 2022), cause
61 protein unfolding/misfolding and modifications (Scharf & Nover 1982; Duncan & Hershey
62 1989; Schroda *et al.* 2015; Rütgers *et al.* 2017; Wang *et al.* 2020), alter cellular
63 metabolites (Hemme *et al.* 2014; Rysiak *et al.* 2021; Jamloki, Bhattacharyya, Nautiyal &
64 Patni 2021), and affect DNA/RNA stability in the nucleus (Kantidze, Velichko, Luzhin &
65 Razin 2016; Su *et al.* 2018). High temperatures also increase reactive oxygen species
66 (ROS) production from chloroplasts and mitochondria (Pospíšil 2016; Janni *et al.* 2020;
67 Niemeyer, Scheuring, Oestreicher, Morgan & Schroda 2021). In addition, high
68 temperatures induce phosphorylation and SUMOylation of heat shock factors (HSFs)
69 which increase the expression of heat shock proteins (HSPs) and other heat response
70 genes (Schroda *et al.* 2015; Guo *et al.* 2016).
71

72 After many years of research, several major questions remain open regarding heat
73 responses in plants, despite of our current understanding as mentioned above (Mittler *et*
74 *al.* 2012; Schroda *et al.* 2015; Vu, Gevaert & De Smet 2019). (1) What are the genes
75 required for heat tolerance? Even with a partial list of such genes, we can better
76 understand heat tolerance in photosynthetic cells and provide engineering targets to
77 make heat tolerant crops. (2) Do different intensities of high temperatures require distinct
78 genes for heat tolerance? High temperatures have different intensities in nature, which
79 have unique physiological effects on photosynthetic cells (Janni *et al.* 2020; Zhang *et al.*
80 2022). Moderate high temperature refers to heat that is slightly above optimal growth
81 temperature, around 35°C for most photosynthetic cells, which causes moderate damage
82 and occurs frequently with prolonged duration in nature (Zhang *et al.* 2022). Acute high
83 temperature refers to heat at or above 40°C, which occurs less frequently but can cause
84 severe damage to cellular processes (Zhang *et al.* 2022). It is unknown whether different
85 high temperatures require unique or overlapping set of genes for thermotolerance. (3)

How does carbon supply affect heat tolerance? Land plants mostly grow photoautotrophically by fixing atmospheric inorganic carbon using photosynthesis, however, there are often various organic carbon sources in the soil. Most green algae can grow both photoautotrophically and mixotrophically with supplied organic carbon. How carbon supply affects heat responses in photosynthetic cells has not been well studied.

The unicellular green alga *Chlamydomonas reinhardtii* (Chlamydomonas throughout) is a powerful model to study heat responses in photosynthetic cells. It has a sequenced, haploid, and simple genome (111 Mb, 17,741 protein-encoding genes) with smaller gene families and lower rates of gene duplication compared to land plants, simplifying genetic analyses (Merchant *et al.* 2007; Karpowicz, Prochnik, Grossman & Merchant 2011). Its 6-8 h doubling time under normal conditions and ability to grow by photosynthesis but also with supplied carbon source is powerful for laboratory experiments and strain maintenance (Harris 2009). Photosynthesis is one of the most heat sensitive functions in plants (Sharkey 2005; Sharkey & Zhang 2010). The photosynthesis in Chlamydomonas is highly similar to land plants (Minagawa & Tokutsu 2015), and its ability to survive on organic carbon enables the maintenance of photosynthetic mutants, making it a superior model to study heat effects on photosynthesis. Additionally, several excellent molecular and genetic tools are available in Chlamydomonas, enabling efficiency gene editing (Shimogawara, Fujiwara, Grossman & Usuda 1998; Greiner *et al.* 2017; Wang *et al.* 2019; Dhokane, Bhadra & Dasgupta 2020) and molecular engineering (Crozet *et al.* 2018; Emrich-Mills *et al.* 2021). Specifically, a mapped, indexed, genome-saturating Chlamydomonas mutant library is available for both reverse and forward genetic screens (Chlamydomonas Library Project, CLiP) (Li *et al.* 2016, 2019).

CLiP mutants each contain at least one unique DNA barcode by the end of the insertional cassette, allowing for high-throughput, quantitative tracking of cell abundance via deep sequencing and growth rate calculation of each individual mutant in pooled cultures under different conditions (Li *et al.* 2016, 2019). Chlamydomonas cells are haploid, so the abundance of a barcode in pooled sequencing data is proportional to the abundance of

117 the CLiP mutant containing this barcode in pooled cultures. If a CLiP mutant is deficient
118 in a gene required for optimal growth under a condition, this CLiP mutant will have
119 reduced growth rate and cell abundance under this condition. The unique DNA barcode
120 is also linked to a mapped insertion site in each mutant, allowing for identification of genes
121 important for growth under a defined condition.
122
123 The Jonikas laboratory, which led the generation of the CLiP mutant library, together with
124 collaborators, employed the CLiP library to screen for mutants deficient in photosynthesis
125 (Li *et al.* 2019) and 121 other different environmental/chemical conditions, including high
126 temperatures (Fauser *et al.* 2022). Fauser et al. (2022) included high temperatures of 30,
127 35, 37°C and also tested the effects of light intensities, CO_2 concentration, and organic
128 carbon availability on heat responses (Supplemental Dataset 1a). The pooled screens by
129 Fauser et al. (2022) have been foundational in using the CLiP mutant library under various
130 screen conditions for functional genomics. They utilized a broad range of experimental
131 conditions for functional prediction of genes with unknown roles and this work has been
132 a pivotal advancement in the field. However, their high temperature screens had several
133 limitations (Supplemental Dataset 1a): (1) They emphasized 30°C heat which is a rather
134 mild high temperature for CC-5325, the background wildtype (WT) strain of the CLiP
135 mutant library (Zhang *et al.* 2014, 2022), and did not include heat at 40°C, which is acute
136 high temperature for CC-5325. (2) They did not include heat at 35°C without carbon
137 supply for parallel comparison with 35°C with carbon supply. (3) Their heat screens were
138 performed in 2 L medium bottles on constant temperature heat blocks (heat stirring
139 plates) without control of culture temperatures, cell density and nutrient supplies, which
140 may complicate the screen results; (4) The CLiP mutants were streaked off the algal
141 plates, inoculated into liquid cultures, and grown under different temperatures directly,
142 without solid to liquid acclimation process before heat treatments, which may increase
143 the false positive rates of heat sensitive mutants; (5) Due to the large-scale nature of their
144 experimental setup, they did not have biological replicates for some of the conditions
145 tested. (6) They did not have heat transcriptome/proteomes to refine their candidate
146 genes identified in the heat screens.
147

148 Our research focused on high temperature conditions using the CLiP mutant library and
149 advanced the high temperature screens by Fauser et al. (2022) to identify a high
150 confidence list of genes important for heat tolerance. Based on the temperature effects
151 on the growth rates of WT CC-5325, we performed pooled CLiP mutant screens under
152 moderate (35°C) and acute high temperature (40°C with and without organic carbon
153 supply in photobioreactors (PBRs) under well-controlled conditions. Our algal cultivation
154 in PBRs had turbidostatic control, which allowed for precise control of growth
155 environments including temperature regulation, heating speed, light intensity, air
156 bubbling, cell density, and, importantly, nutrient supply. In our cultivation method, we can
157 isolate the effects of high temperatures on algal cells and minimize the complications from
158 other environmental factors, such as nutrient depletion or light shading. Additionally, we
159 leveraged our recently published Chlamydomonas transcriptome/proteome data under
160 35°C and 40°C to increase confidence in heat tolerance genes (HTGs) identified from our
161 pooled mutant screens. If a gene or protein is induced during heat and a mutant deficient
162 in this gene has heat sensitive phenotype, we have high confidence that this gene has a
163 role in thermotolerance. Furthermore, we developed a triangulation approach to combine
164 CLiP pooled screens, transcriptome/proteomics data, and functional annotations to
165 identify high confidence genes with known and novel roles in heat tolerance. Finally, our
166 ortholog analysis revealed that many of the HTGs identified in Chlamydomonas are
167 conserved in land plants and *Arabidopsis thaliana* (Arabidopsis throughout) mutants
168 deficient in the orthologous gene of a Chlamydomonas HTG were heat sensitive. Our
169 research can provide engineering targets to improve thermotolerance in both green algae
170 and land plants.
171
172 **Materials and Methods**
173 **Algal cultivation**
174 All Chlamydomonas liquid cultivation used in this paper was conducted in
175 photobioreactors (PBRs) as described before (Zhang *et al.* 2022) with minor
176 modifications. Algal cultures were grown in standard Tris-acetate-phosphate (TAP, with
177 acetate, an organic carbon source) or Tris-phosphate (TP, without acetate) medium with
178 modified trace elements (Kropat *et al.* 2011) in 1-L PBRs (Photon System Instruments,

179 FMT 150/1000-RB). Cultures were illuminated with constant 100 μmol photons
180 m^2 s^{-1} light (50% red: 50% blue), mixed by bubbling with filtered air. After inoculation,
181 cultures grew to a target cell density of 2×10^6 cells/mL in log-phase growth at 25°C. Then,
182 the target cell density was maintained turbidostatically using OD_{680} (monitored every 1
183 min automatically) by allowing the culture to grow to 8% above the target cell density
184 before being diluted to 8% below the target cell density with fresh medium provided
185 through peristaltic pumps. Through the turbidostatic mode, the PBR cultures had constant
186 nutrient supply, controlled cell density, and exponential growth between dilution events.
187 The OD_{680} measurements during exponential growth phases in between dilution events
188 were $\log_2$ transformed, and the relative growth rate was calculated using the slope of
189 $\log_2(OD_{680})$, while the inverse of the slope yielded the doubling time of the culture (Zhang
190 *et al.* 2022). Different treatments (different heat and medium type) were conducted in
191 individual PBRs. For WT CC-5325 cultures, cells were first acclimated at 25°C until
192 reaching steady growth rates before switching to different high temperatures.
193
194 For pooled screens, the CLiP mutant library was pooled as described before (Fauser *et*
195 *al.* 2022) with minor modifications. The CLiP library was replicated using a Singer RoToR
196 robot (Singer Instruments, 704) on 384-format 1.5% TAP agar plates and grown in dark.
197 Five-day-old fresh plates with the CLiP mutant library were pooled using sterile glass
198 spreaders in liquid TAP medium, vortexed to break the colonies, grown on shaker in dark
199 at room temperature overnight before being inoculated into PBRs the next day. This gave
200 cells time to acclimate from solid agar to liquid cultures before inoculation to PBRs. Pooled
201 CLiP liquid cultures were diluted using TAP or TP medium before inoculated into PBRs
202 at 25°C in TAP or TP medium (initial cell density around 1×10^6 cells mL^{-1}), acclimated at
203 25°C in light for 2 days to reach steady growth rates before the start of heat treatments
204 at 35°C or 40°C. Acclimation at 25°C in light was used to reduce false-positive heat
205 sensitive mutants. The heat of 35°C lasted 4 (TAP) or 5 (TP) days and the heat of 40°C
206 lasted 2 days because the algal cultures would not survive if heated at 40°C for longer.
207 After 40°C heat, cultures recovered at 25°C for 3 days. Algal cultures of pooled mutants
208 (2 x 50 mL) were harvested before and after the heat treatments, or by the end of recovery

209 using centrifugation at 4°C for 5 min. Cell pellets were frozen in liquid nitrogen and stored
210 at -80°C before DNA extraction and barcode amplification.
211
212 **DNA extraction and sequencing**
213 Genomic DNA was extracted for DNA barcode amplification as described before (Li *et al.*
214 2016) with minor modifications. Frozen cell pellets (from one copy of 50 mL cultures) were
215 mixed with 800 µL of SDS-EDTA buffer (1% SDS, 200 mM NaCl, 20 mM EDTA, 50 mM
216 Tris-HCL, pH 8) and separated into two equal aliquots for downstream processing. Then,
217 500 µL of 24:25:1 phenol:chloroform:isoamyl alcohol (Sigma, P2069-400ML) was added
218 to each tube. Samples were vortexed for 2 min, centrifuged for 5 min at 10,000 g, and the
219 aqueous phase was aliquoted into a new PhaseLock tube (VWR, Cat No. 10847-800),
220 added with 1.6 µL of 100 mg/µL RNaseA (ThermoFisher Scientific, Cat. No. 1209102),
221 and incubated at 37°C for 30 min. The phenol/chloroform DNA extraction was repeated
222 three additional times. After the final extraction, samples were transferred to a new 1.5
223 mL tube and 2.5 volumes cold 100% ethanol was added. Samples were incubated in a -
224 20°C freezer for 1 h then centrifuged at 16,000 g for 20 min at 4°C. Supernatant was
225 decanted and pellets were washed in 1 mL cold 70% ethanol. Supernatant was decanted,
226 pellets dried for 30 min at room temperature and DNA pellets were resuspended in 50 µL
227 molecular grade water. Like samples were combined into a single tube then quantified by
228 high sensitivity DNA Qubit (ThermoFisher scientific, Cat. No. Q32854).
229
230 **DNA barcode amplification and sequencing**
231 DNA barcodes were amplified as described before (Li *et al.* 2016) with minor
232 modifications. Barcodes from the 5' and 3' side of the insertional cassette were amplified,
233 sequenced, and processed separately. PCR reactions of 50 µL were prepared as follows:
234 PCR 5' side barcodes: 17 µL molecular grade water, 10 µL GC buffer, 5 µL DMSO, 1 µL
235 dNTPs at 10 mM, 1 µL $MgCl_2$ at 50 mM, 2.5 µL each primer at 10 µM, 1 µL Phusion
236 HotStart polymerase, and 10 µL DNA at 12.5 ng/µL. Samples were amplified using the
237 following PCR cycle for 5' side barcodes: 98°C for 3 min, 10 cycles of 98°C for 10 s, 58°C
238 for 25 s, 72°C for 15 s, 10 cycles of 98°C for 10 s, 72°C for 40 s. PCR for 3' side barcodes:
239 16 µL molecular grade water, 10 µL GC buffer, 5 µL DMSO, 1 µL dNTPs at 10 mM, 2 µL

240 $MgCl_2$ at 50 mM, 2.5 µL each primer at 10 µM, 1 µL Phusion HotStart polymerase, and
241 10 µL DNA at 12.5 ng/µL. Samples were amplified using the following PCR cycle for 3'
242 side barcodes: 98°C for 3 min, 10 cycles of 98°C for 10 s, 63°C for 25 s, 72°C for 15 s, 9
243 cycles of 98°C for 10 s, 72°C for 40 s.
244
245 PCR products were cleaned and concentrated using the MinElute Gel Extraction kit
246 (Qiagen, Cat. No. 28606). Purified product was separated by gel electrophoresis using a
247 1.5% agarose gel performed at 130 V for 65 min. PCR bands of 235 bp (5' side barcodes)
248 and 209 bp (3' side barcodes) were excised from agarose gel and extracted with the
249 MinElute Gel Extraction kit. Final purified DNA was eluted with 20 µL elution buffer. DNA
250 concentration was quantified using Qubit and the quality of DNA was visualized using 8%
251 TBE gel (Invitrogen, Cat. No. EC62152BOX) performed at 230 V for 30 min. Gel was
252 stained for 5 min with SYBRGold (ThermoFisher Scientific, Cat. No. S11494) prior to
253 image acquisition.
254
255 Because samples were pooled together for sequencing, barcode amplification primers
256 contained unique indexes for downstream identification in the data analysis pipeline
257 (Supplemental Dataset 1b). Prior to sequencing, eight DNA samples were pooled
258 together for a total of 23.75 ng of each DNA sample in a final volume of 25 µL. Samples
259 were sequenced at the Department of Energy Joint Genome Institute (DOE JGI) using
260 the Illumina Hi-seq platform. The prepared libraries were quantified using KAPA
261 Biosystems' next-generation sequencing library qPCR kit and ran on a Roche LightCycler
262 480 real-time PCR instrument. Sequencing of the flowcell was performed on the Illumina
263 NextSeq500 sequencer using NextSeq500 Mid Output kits, v2, following a 1 x 50 indexed
264 run recipe utilizing a custom sequencing primer. Reads were mapped to each DNA
265 sample using the index code contained in the PCR amplification primer. Each DNA
266 sample had an average of 27 million and the minimum number of reads was 8 million.
267
268 **Barcode abundance quantification and normalized read count cutoffs**
269 From the deep sequencing reads, common cassette sequences were trimmed using
270 Geneious v10.1.3, leaving only the unique DNA barcodes. The number of reads from

271 each unique DNA barcode was quantified and the total number of reads for each sample
272 was normalized to 100 million. The unique DNA barcodes were mapped to the CLiP
273 mutant library with no mismatch bases allowed. Minimum cutoffs of normalized barcode
274 read count were implemented: ≥150 normalized reads in all T1 samples (beginning of the
275 treatment period for control and the high temperature treatment) and ≥1 read from T3a or
276 T3b (end of the screens) in the control condition (Figure S1). Barcodes from heat-
277 compromised individuals were required to have ≥1 read in T3a or T3b of the high
278 temperature treatments. Barcodes from heat-depleted individuals had 0 reads in at least
279 1 biological replicate at T3a or T3b of the high temperature treatments.
280

281 **Principal component analysis**

282 Principal component analysis was performed on normalized read counts from all
283 barcodes in all biological replicates using the R package FactoMineR (Lê, Josse &
284 Husson 2008).
285

286 **Growth rate calculations**

287 The growth rate from each individual barcode was calculated using the following equation:

288
$$\frac{\left(\left[\frac{\boldsymbol{log_2}\left(\boldsymbol{d}/\boldsymbol{c}\right)}{\boldsymbol{N}}\right]+\mathbf{1}\right)}{\boldsymbol{R}}$$

289 Where d represents the normalized reads at T3a or T3b (end of screens), c represents
290 the normalized reads at T1 (start of screens), and N represents the estimated number of
291 generations that occurred in each given biological replicate (see Supplemental Dataset
292 1c). These calculations were performed for all barcodes in a biological replicate, then
293 growth rates were divided by R, the mean growth rate of all mutants in the biological
294 replicate to normalize for effects of different treatments. Each mutant was compared to
295 all other mutants in the same biological replicate; thus, the calculated growth rate of each
296 mutant is relative to the whole mutant pool. Relative growth rates were calculated for each
297 barcode in control and high temperature treatments. The mean doubling time of each
298 treatment was calculated based on the exponential increase of OD_{680}, as mentioned
299 above. The number of generations that occurred in each biological replicate was

300 estimated by the duration of the experiment divided by the mean doubling time
301 (Supplemental Dataset 1c). The mean growth rate of all mutants in a biological replicate
302 is inverse of the doubling time. The cell cycle was arrested in 40ºC (Zhang *et al.* 2022),
303 thus for 40ºC treated cultures, we assume zero generations occurred during the 2-day
304 40ºC heat, therefore only estimated the number of generations that occurred during the
305 25ºC recovery period following the 40ºC heat treatment. Mutants that were depleted by
306 the end of the 2-day 40ºC heat were included as heat-depleted mutants (see below).
307

308 **Growth rate validation of individual mutants in monocultures**

309 Ten individual CLiP mutants were selected for monoculture phenotyping. The identities
310 of these mutants were verified by PCR using primers that bind to the cassette or flanking
311 genomic regions (Supplemental Dataset 1b) as described before (Li *et al.* 2016). PCR
312 products were sequenced for confirmation. Mutants were individually grown in PBRs as
313 mentioned above. Cultures were acclimated for 4 days at 25ºC before raising the
314 temperature to 35ºC for 4 days. The exponential increase of OD_{680} was used to determine
315 the doubling time (Td) of the culture, which was then used to calculate the growth rate
316 (1/Td) as described above. For the growth rate at 25ºC, doubling times from the last 24
317 hours of 25ºC before changing to 35ºC were used to calculate the average pre-heat
318 growth rate. The growth rate at 35ºC was calculated from all doubling times from 6 hours
319 after temperature increase to 35ºC to the end of 35ºC heat. Doubling times from the first
320 6 hours of 35ºC heat treatment tended to be inconsistent as the culture adjusted to the
321 higher temperature. A normalized growth rate was then calculated by dividing the mutant
322 growth rate by the growth rate of WT CC-5325 (CLiP background) for each temperature
323 condition.
324

325 **Identification of heat-compromised and heat-depleted mutants**

326 Heat-compromised individuals are required to have a mean normalized growth rate at
327 25ºC ≥0.95 (normal growth) and a mean normalized growth rate at high temperature of
328 ≤0.8 (compromised growth) (Figure S2a-f). Additionally, using the normalized growth
329 rates of two biological replicates at each treatment condition, we performed a student's
330 one-sided t-test of unequal variance for each barcode that met normalized read count

331 cutoffs. Significance was defined as $p < 0.05$ and t-value in the 95th percentile (Figure
332 S2g-j). Heat-depleted individuals were also required to have a mean normalized growth
333 rate at 25°C ≥0.95 (normal growth), but because they were completely depleted from at
334 least one biological replicate at high temperature, a growth rate could not be calculated.
335 Heat tolerance genes (HTGs) were defined as those with at least one heat-compromised
336 or heat-depleted mutant. All the pooled screen data with gene IDs, mutant IDs,
337 phenotypes is in Supplemental Dataset 2.
338
339 **Comparisons between conditions**
340 To compare the HTGs between conditions, we filtered the dataset for only those genes
341 that were represented by at least one mutant in all four treatment conditions.
342 Comparisons between conditions were visualized using UpSetR (Conway, Lex &
343 Gehlenborg 2017).
344
345 **MapMan functional enrichment**
346 Functional enrichment analysis was performed using MapMan for different combinations
347 of conditions including: all HTGs from all conditions, and HTGs overlapping between both
348 TAP conditions or both TP conditions or both 35°C conditions or both 40°C conditions, or
349 all four conditions. Gene lists were expanded such that one gene can be associated with
350 multiple MapMan functional terms. Enrichment was assessed using a Fisher's Exact Test,
351 FDR < 0.05 (Venn & Mühlhaus 2022; Venn *et al.* 2022; Benjamini & Hochberg 01/1995).
352
353 **Transcriptome and proteome comparisons**
354 HTGs from all four conditions were compared with previously published RNA-seq data
355 from WT (CC-1690) Chlamydomonas cells treated for 24 h at either 35°C or 40°C followed
356 by a 48 h recovery period at 25°C in TAP medium (Zhang *et al.* 2022). Differentially
357 expressed genes were sorted into heat induced genes (HIGs, upregulated in ≥1 time point
358 during the high temperature period). HIGs were filtered for genes that had ≥1 CLiP mutant
359 present in pooled mutant screens. HTGs were also filtered for those genes that met
360 minimum read count cutoffs in the RNA-seq dataset. Overlaps between HTGs and HIGs,
361 were quantified, and enrichment was determined using a Fisher's exact test, FDR < 0.05.

362 These RNA-seq data also included modules of genes with similar expression profiles
363 using Weighted Correlation Network Analysis (WGCNA) (Langfelder & Horvath 2008;
364 Zhang *et al.* 2022). HTGs from the TAP-35°C, TAP-40°C, and the aggregated HTGs from
365 all 4 conditions were sorted within these modules. For modules that contained more HTGs
366 than would be expected by random chance from these groups (Fisher's exact test, FDR
367 < 0.05), MapMan functional enrichment analysis was performed on the overlapping
368 WGCNA module list and HTG list as described above.
369
370 **Heat sensitivity assay of Arabidopsis mutants**
371 Arabidopsis T-DNA insertional mutants were obtained from the Arabidopsis Biological
372 Resource Center (ABRC): *Athmt-1* (SAIL_114_G09) and *Athmt-2* (SALK_106875C), and
373 the positive control *Athot1* (SALK_066374C). Homozygous insertional mutants were
374 verified by PCR as described before (Sessions *et al.* 2002; Alonso *et al.* 2003) (see
375 Supplemental Dataset 1b for primer sequences). WT Col-0 seeds were from Dr. Dan Lin
376 at the Donald Danforth Plant Science Center. Seeds from homozygous lines were used
377 for heat sensitivity assays. Seeds were sterilized in 500 µL 20% bleach with 1 µL 20%
378 Tween20 followed by five washes using sterile water, then plated on MS-sucrose plates
379 (0.5X Murashige and Skoog (MS) salts, 1% sucrose), stratified for 3 days in dark at 4°C,
380 then grown in constant white light of 115 µmol photons m^2 s^{-1} at 25°C in a Conviron
381 growth chamber. After 7 days of growth, 3 biological replicates of seedlings were heated
382 at 41°C for 45 min in a pre-warmed water bath. Heat treated plates were returned to the
383 25°C growth chamber mentioned above for an additional 7 days for recovery before
384 imaging. Mean plantlet area was measured using ImageJ by dividing the total plantlet
385 area of each genotype by the number of seeds that germinated for that genotype. Mutant
386 plantlet area was normalized to that of Col-0 on the same plate. Statistical significance of
387 mutants compared to WT on the same plates was assessed with a student's one-sided t-
388 test of unequal variance. Control plates were sterilized and stratified as described above,
389 then grown at 25°C in a Conviron growth chamber as mentioned above for 14 days. No
390 observable phenotype differences were found between mutants and Col-0 under 25°C .
391 Gene models for *CrHMT* and *AtHMT* were generated using the Gene Structure Display
392 Server (GSDS2.0) (Hu *et al.* 2015).

393

394 **Results**

395 **Pooled mutant screens were conducted at moderate and acute high temperatures**

396 We first grew CC-5325, the WT background strain of the CLiP mutant library, in
397 photobioreactors (PBRs) under well-controlled conditions to test our heat screen
398 conditions. Cells were grown in PBRs under constant light in either Tris-acetate-
399 phosphate (TAP) medium (contains acetate, the organic carbon source), or Tris-
400 phosphate medium (TP, no acetate) under different temperatures. With supplied carbon,
401 the growth rate of CC-5325 increased at 30ºC and 35ºC but decreased at 40ºC as
402 compared to 25ºC (Figure 1a). The increased growth rates at 30ºC and 35ºC were
403 abolished without supplied organic carbon source, although the cultures were still very
404 sensitive to 40ºC. We defined 35ºC as moderate high temperature, and 40ºC as acute
405 high temperature. We performed genome-wide, quantitative, pooled mutant screens in
406 PBRs using the CLiP mutant library at 25ºC, 35ºC, and 40ºC with or without carbon source
407 (Figure 1b). Algal cultures were harvested at the beginning (T1) and end (T3a or T3b) of
408 the treatment period for DNA extraction, barcode quantification by deep sequencing, and
409 growth rate calculation for each mutant (Figure 1c). Principal component analysis of
410 normalized read abundance from all barcodes in each sample showed high reproducibility
411 between biological replicates (Figure 1d, Figure S1). PC1 explains 40.8% of the dataset
412 variance and separates samples based on medium condition, with and without carbon
413 supply. PC2 explains 11.2% of the dataset variance and separates samples based on
414 both temperature treatments and time points.

415

416 **Growth rates can be calculated consistently**

417 We calculated the growth rates of each mutant using the normalized read counts from
418 barcodes at the beginning and end of the treatment period (see Methods). Growth rates
419 were highly reproducible between two different barcodes from the same mutant
420 (amplified, sequenced, and processed separately, therefore serving as internal controls
421 for pipeline reproducibility), as well as between biological replicates (Figure 2a-d).
422 Furthermore, we validated the growth rates of 10 individual CLiP mutants from the pooled
423 mutant screens at 25ºC or 35ºC treatment condition in PBRs using monocultures (Figure

424 2e). Monoculture growth rates were highly consistent with those calculated from pooled
425 mutant screens.
426
427 **Heat-compromised and heat-depleted mutants were identified in the screens**
428 We identified heat-compromised and heat-depleted mutants using growth rates for each
429 of the 4 screen conditions (Figure 3). Heat-compromised mutants have mean growth rate
430 at 25°C ≥ 0.95, mean growth rate at high temperature (35°C or 40°C) ≤ 0.8, $p < 0.05$ and
431 t-value in the 95th percentile (student's one-sided t-test of unequal variance) (Figure 3,
432 Figure S2, Supplementary Dataset 1d). Heat-depleted mutants have mean 25°C growth
433 rate ≥ 0.95 but were absent by the end of the treatment period in at least one high
434 temperature replicate (Figure 3, Supplementary Dataset 1d). The aggregated lists of heat-
435 compromised and heat-depleted mutants are referred to as heat sensitive mutants.
436 Because all heat sensitive mutants have normal growth rates at 25°C, they specifically
437 have growth defects under high temperature treatments.
438
439 **We investigated the aggregated features of the heat sensitive mutants**
440 All CLiP mutants have mapped insertion sites with insertion features and confidence
441 levels (Li *et al.* 2016). The distribution of both insertion features and confidence levels
442 (Figure 4a, b) of heat-sensitive mutants is similar to all CLiP mutants present in our
443 screens. While most genes had a single mutant allele that was heat sensitive, 5-11% of
444 genes had two or more heat sensitive mutant alleles in a single condition (Figure 4c).
445 Genes with multiple independent heat-sensitive mutant alleles have a high likelihood of
446 being required for thermotolerance. Because each unique DNA barcode is linked to a
447 disrupted gene in a CLiP mutant (Li *et al.* 2016, 2019), based on the identified heat
448 sensitive mutants, we generated a list of genes (4,529) with potential roles in heat
449 tolerance, defined as **Heat Tolerance Genes (HTGs)** (Supplemental Dataset 1d). Each
450 HTG has at least one heat-sensitive mutant. Next, we investigated the predicted
451 subcellular localizations of the aggregated list of HTGs from all conditions using published
452 predictions (Venn & Mühlhaus 2022; Venn *et al.* 2022). We found that significantly more
453 HTGs have predicted localization in the secretory pathway than expected by random
454 chance (Fisher's Exact Test, $p < 0.01$) (Figure 4d). Of the HTGs with predicted subcellular

455 localizations, 35.17% (818 genes) had proteins predicted to localize in the secretory
456 pathway. Additionally, we identified at least 25 genes with known roles in thermotolerance
457 in our list of HTGs, including 14 chaperone proteins, 9 members of the algal carbon
458 concentrating mechanism, and both copies of rubisco activase (RCA) (Supplemental
459 Dataset 1e). We identified 2,510 (48%) of HTGs that have no function annotation,
460 suggesting novel genes with putative roles in thermotolerance. Furthermore, we identified
461 75 HTGs as transcription factors (Jin *et al.* 2017) (Supplemental Dataset 1f), highlighting
462 the extensive and complex regulation required for coordinating high temperature
463 responses.
464
465 **We identified overlapping HTGs between conditions**
466 We next investigated the overlapping HTGs between the four treatment conditions. For
467 this analysis, we only considered those HTGs that were represented by at least one
468 mutant in all four treatment conditions. Consistent with principal component analysis
469 which showed medium treatment had the largest effect on dataset variance (Figure 1d),
470 we found that many HTGs are shared within medium treatments, with 401 genes uniquely
471 having heat-sensitive mutants in TAP conditions and 48 genes uniquely having heat-
472 sensitive genes in TP conditions (Figure 5a). When comparing temperature treatments,
473 we found 189 HTGs unique to 35°C treatment groups and 172 genes unique to 40°C
474 treatment groups.
475
476 To better understand the biological functions of HTGs, we performed functional
477 enrichment analysis using MapMan annotations (Figure 5b, Supplemental Dataset 3a-f).
478 In the aggregated list of HTGs from all conditions, we found significantly enriched
479 MapMan terms for signaling, chromatin remodeling factors, and callose. We also
480 investigated the functional enrichment of HTGs in overlapping medium and temperature
481 conditions. For those HTGs found in both TAP conditions (TAP-35°C and TAP-40°C),
482 there were many significantly enriched MapMan terms including calcium transport, iron
483 hydrogenases, protein degradation, lipid metabolism, glycolysis, and cell motility.
484 Interestingly, the glycolysis MapMan terms are unique to TAP screens, with the supplied
485 organic carbon source. There was not extensive functional enrichment for HTGs found in

486 both TP conditions, except for cell motility. For HTGs found in both 35°C conditions,
487 calcium signaling, iron hydrogenases, ARR transcription factors, and cell motility were
488 among the significantly enriched MapMan terms. For HTGs found in both 40°C conditions,
489 calcineurin-like phosphoesterases, methionine-tRNA ligases, 30S ribosomal subunit, and
490 cell motility were among the significantly enriched MapMan terms. Finally, we found 56
491 genes with at least one heat-sensitive mutant in all four treatment conditions (Figure 5a,
492 Supplemental Dataset 1g), which are significantly enriched for MapMan terms related to
493 nutrient/sugar signaling and cell motility (Supplemental Dataset 3f).
494
495 **Some heat tolerance genes (HTGs) may be also involved in other stresses**
496 We defined HTGs with high confidence heat sensitive mutants (HSMs) as those that
497 either (a) had at least two HSMs in one or more treatment conditions or (b) had one HSM
498 with a heat sensitive phenotype in at least two conditions. We next investigated the
499 behavior of these 1,693 HTGs with high confidence HSMs in other pooled screen
500 conditions conducted by Fauser et al. (2022) to see if these HTGs are heat-specific.
501 Previous pooled screens investigated the behavior of CLiP mutants in approximately 121
502 different screen conditions (Fauser *et al.* 2022), which we sorted into 16 broad categories
503 (Figure S3). Fauser et al. (2022) used two significance thresholds for analysis, FDR < 0.3
504 and FDR < 0.05. We reported comparisons for the FDR < 0.3 threshold (Figure S3) and
505 included comparisons for both thresholds in Supplemental Dataset 1i & j. For the 16 broad
506 categories, we reported the percentage of genes identified by Fauser et al. (2022) with
507 sensitive mutants that are also high confidence HTGs in our work. Of our 1,693 HTGs
508 with high confidence heat sensitive mutants, we found that 183 also had CLiP mutants
509 there were sensitive to other screen conditions by Fauser et al. (2022) (FDR < 0.3),
510 meaning these genes may be also involved in other stresses. Out of the 39 genes with
511 putative roles in heat tolerance that were identified in the heat screens of Fauser et al.
512 2022 (FDR < 0.3), 10 are present on our HTG list with high confidence HSMs (16 overlap
513 if considering all HTGs) (Supplemental Dataset 1i&j).
514
515 **We investigated HTGs using high temperature transcriptomes and proteomes**

516 If a gene is up-regulated at the transcript and/or protein level during high temperatures
517 and disruption of this gene results in a heat sensitive phenotype, this gene likely has an
518 important role in thermotolerance. Thus, we compared our HTGs with our previously
519 published transcriptomes and proteomes in WT Chlamydomonas with heat treatments
520 under the same cultivation conditions (Zhang *et al.* 2022). Our previous RNA-seq analysis
521 identified differentially regulated genes and proteins during 24-hours of moderate (35°C)
522 or acute (40°C) high temperatures followed by 48-hours of recovery at 25°C (Zhang *et al.*
523 2022). Our previous RNA-seq identified 3,960 heat induced genes (HIGs), up-regulated
524 in at least one time point during the heat treatments of 35°C or 40°C, and 3,503 of them
525 were also present in our pooled screen experiments. Among our HTGs, 4,308 met the
526 minimum read count cutoffs used in the RNA-seq experiment. We found 1,224 genes
527 overlapping between the HIG and HTG lists, significantly more than expected by random
528 chance (Fisher's exact test, $p < 0.001$) (Figure 6a). Because some genes were
529 differentially regulated at the protein level but not the transcript level in our previous data,
530 we were interested in identifying the overlaps between heat induced proteins (HIPs, 549
531 proteins) and HTGs (Figure 6b). We found 111 genes that were both HIPs and HTGs.
532 Unlike the overlap between HTGs and HIGs, the overlap between HTGs and HIPs were
533 significantly de-enriched below what would be expected by random chance (111
534 observed vs 138 expected). This proteomics dataset was generated by untargeted mass
535 spectrometry, resulting in identification of primarily highly abundant proteins. However,
536 the distribution of HTGs is not over-represented for highly abundant proteins, likely
537 because highly abundant proteins may also be performing important functions under
538 control temperatures. Our HTGs are required to have mutants with normal growth rates
539 at 25°C but reduced growth rates during heat treatments.
540
541 Our previous transcriptome analyses also identified common transcriptional patterns
542 during and after high temperatures using weighted correlation network analysis (WGCNA)
543 (Zhang *et al.* 2022). Interestingly, the HTGs identified in our pooled screens were non-
544 randomly distributed among the WGCNA modules (Figure 6c). Of particular interest is
545 transcriptome module 1 (TM1), which contains 559 genes that are both in TM1 and have
546 at least one mutant in our pooled screens (Supplemental Dataset 1k). These genes have

547 peak expression at the beginning of high temperature and most genes with known roles
548 in thermotolerance (e.g., HSPs) have this transcriptional pattern. Of those 559 genes,
549 249 were also identified as HTGs in our pooled screens (defined as TM1-HTGs).
550 Furthermore, 129 and 95 of these TM1-HTGs have heat sensitive mutants in the TAP-
551 40ºC and TAP-35ºC screen condition, respectively. These subsets are all significantly
552 enriched above random chance ($p < 0.05$, Fisher's Exact Test). We performed MapMan
553 functional enrichment analysis on these TM1-HTGs to gain further understanding of their
554 functions (Supplemental Dataset 3g). MapMan terms relating to heat stress, protein
555 folding, PSII biogenesis, thioredoxins, and lipid metabolism were significantly enriched.
556 Half of TM1-HTGs have unknown functions, and these genes are of particular interest for
557 future study. HTGs were also overrepresented in TM3, which contains 459 genes that are
558 present in the pooled screens, and 178 of them were HTGs ($p < 0.05$, Fisher's Exact Test)
559 (TM3-HTGs) (Supplemental Dataset 1k). These genes have peaks in expression during
560 both the early high temperature and early recovery periods. The TM3-HTGs were
561 significantly enriched for DNA repair, calcium transport, protein degradation, and
562 thioredoxins (Supplemental Dataset 3h).
563
564 **A triangulation approach identified high confidence heat tolerance genes (HTGs)**
565 To increase the confidence in our putative HTGs, we leveraged our previously published
566 transcriptome and proteome data under high temperatures along with MapMan functional
567 annotations. By triangulating these three datasets, we have narrowed the candidate list
568 of HTGs to those with our highest confidence. We required high confidence HTGs to meet
569 two of the three criteria below: (Figure 7a). (A) having high confidence heat sensitive
570 mutants (HSMs) in our pooled mutant screens (1,693 genes, HTGs that had at least one
571 heat sensitive mutant in at least two conditions or at least two heat sensitive mutant alleles
572 in any one condition in our pooled screens). (B) The gene was induced by heat in our
573 previously published RNA-seq or proteomics data (4,344 genes) (Zhang *et al.* 2022). (C)
574 The gene has a MapMan annotation related to a pathway known to be involved in heat
575 tolerance or affected by high temperatures (1020 genes, Supplemental Dataset 3j),
576 including heat response (e.g., HSPs), protein folding, lipid metabolism, calcium signaling,
577 photosynthesis, the carbon concentrating mechanism, redox, and other stress responses.

578 Using this triangulation approach, we identified 933 genes that we define as high
579 confidence HTGs (Supplemental Dataset 1l); 43 of these genes meet all three of the
580 criteria used, including rubisco activases 1 and 2 (RCA1/2), the CCM subunits LCI1 and
581 PHC25, heat shock protein HSP70A, and thioredoxin TRXf2 (Supplemental Dataset 1m).
582
583 Of particular interest are the 504 genes that meet criteria A and B (heat sensitive mutants
584 and heat induced transcripts/proteins) because they have two independent experimental
585 datatypes pointing to a role in thermotolerance. Since this category has no requirement
586 for functional annotation, 282 genes out 504 genes (56%) have no MapMan annotations,
587 suggesting novel players in thermotolerance. The remaining 222 genes were significantly
588 enriched for signaling, transcription regulation, redox, lipid metabolism, starch synthases,
589 and more (FDR < 0.05).
590
591 There were 113 genes in the intersection between A and C (heat sensitive mutants and
592 MapMan annotations). These genes do not necessarily have increased transcript/protein
593 levels under high temperatures. We expect some genes to encode proteins that have
594 important functions in thermotolerance but may not change transcript/protein abundance,
595 or via other post-translational regulation. For example, some proteins may undergo
596 conformational changes to activate and not need to increase in abundance to perform
597 their role in thermotolerance.
598
599 The intersection between B and C (heat-induced transcripts/proteins and in MapMan
600 annotation) contained 402 genes. There are several reasons why these genes would not
601 be identified in the pooled screen analyses but could still be of great interest. (1) The gene
602 has redundant functionality with another gene, resulting in lack of phenotype in single
603 mutants; (2) the gene may not be represented by knockout mutants in the pooled screen
604 because it is an essential gene, as is the case with the master regulator of heat
605 responses, HSF1; (3) the CLiP mutants have insertions in 3'UTR or introns, thus no
606 observable phenotypes in our pooled screens.
607

608 Additionally, we overlayed our set of 933 high-confidence HTGs with the ChlamyNet
609 dataset, a transcriptional network based on expression patterns of Chlamydomonas
610 under various conditions (Romero-Campero, Perez-Hurtado, Lucas-Reina, Romero &
611 Valverde 2016). We found that our high-confidence HTGs were overrepresented in three
612 ChlamyNet modules named "stress response and protein folding", "protein
613 phosphorylation and carbon/nitrogen metabolism", and "GTPase activity and autophagy"
614 (Figure 7b), supporting the important roles of our HTGs in thermotolerance.
615
616 **Our research in Chlamydomonas can inform orthologous HTGs in land plants**
617 We investigated the conservation of 933 high-confidence HTGs that met triangulation
618 cutoffs in the green lineage. We identified one-to-one, one-to-many, many-to-one, and
619 many-to-many orthologs with eight species using the JGI In.Paranoid dataset (Remm,
620 Storm & Sonnhammer 2001) (Figure 8a). For most species investigated, approximately
621 half of the high-confidence Chlamydomonas HTGs had orthologs in land plants,
622 suggesting the HTGs identified in Chlamydomonas can be used to infer the function of
623 these HTGs in land plants and provide engineering targets to improve thermotolerance in
624 crops. Of the 933 high confidence HTGs, 173 had a one-to-one orthologous relationship
625 with a gene in the model plant *Arabidopsis thaliana* (Arabidopsis) and 49 of these 173
626 genes (28%) were also up-regulated at the transcript level in Arabidopsis during high
627 temperatures (42°C for 7 h) (Balfagón *et al.* 2019) (Supplemental Dataset 1n).
628
629 To demonstrate that our results from Chlamydomonas can be broadly applied in land
630 plants, we investigated the heat sensitivity of Arabidopsis mutants disrupted in orthologs
631 of high confidence HTGs identified in Chlamydomonas. We required these HTGs to meet
632 the following criteria: (1) there is a one-to-one homolog in Arabidopsis with a
633 Chlamydomonas high-confidence HTG; (2) there are at least two heat sensitive mutants
634 in this HTG in Chlamydomonas; (3) the transcript or protein of this HTG is up-regulated
635 during high temperature in Chlamydomonas (Zhang *et al.* 2022); and (4) the
636 corresponding Arabidopsis transcript is up-regulated during high temperature (Balfagón
637 *et al.* 2019). Among HTGs that meet these criteria, we identified one Chlamydomonas
638 HTG (Cre11.g467752) and its one-to-one ortholog in Arabidopsis (AT4G26240). The

639 Arabidopsis gene is annotated as a putative histone-lysine N-methyltransferase (HMT) at
640 The Arabidopsis Information Resource (TAIR) website, though detailed functional
641 characterization of these two genes is lacking in both organisms.
642
643 *CrHMT* was up-regulated at the transcript level in both early heat and early recovery in
644 40ºC, and also during early recovery following 35ºC (Figure 8b). Three CLiP mutant
645 alleles in *CrHMT* were heat sensitive in our pooled mutant screens (Figure 8c, d). We
646 obtained two insertional mutant alleles in *AtHMT* (Figure 8e) and tested their heat
647 sensitivity as compared to their WT background, Columbia (Col-0), as well as a well-
648 documented mutant with a heat sensitive phenotype, *hot-1*, which is mutated in the large
649 heat shock protein HSP101 (Queitsch, Hong, Vierling & Lindquist 2000; Larkindale, Hall,
650 Knight & Vierling 2005; Cha *et al.* 2020). After a 45-minute heat treatment at 41ºC
651 followed by 7-day recovery at 25ºC, we found *hot1* and *hmt-2* mutants had significantly
652 lower mean plantlet areas 7 days at 41ºC as compared to WT (Figure 8f, g).
653
654 **Discussion**
655
656 We performed genome-wide, quantitative, pooled mutant screens under moderate (35ºC)
657 and acute (40ºC) high temperatures in medium with either organic carbon (TAP) or no
658 organic carbon (TP) using the Chlamydomonas CLiP mutant library. Through these
659 screens, we identified putative heat tolerance genes (HTGs) in each condition and
660 overlapping conditions. By overlaying these data with previously published
661 transcriptomics and proteomics data during high temperatures and MapMan functional
662 annotations, we report a list of 933 high confidence HTGs in Chlamydomonas, about 50%
663 of which are conserved in land plants and are prime targets for improving the heat
664 tolerance in green algae and land plants. Arabidopsis mutants deficient in the ortholog of
665 a Chlamydomonas HTG were heat sensitive, providing evidence that our results in
666 Chlamydomonas can be used to infer thermotolerance genes in land plants.
667
668 **Our research enables high-sensitive discovery of novel heat tolerance genes**
669 Previous pooled screens utilizing the CLiP mutant library employed a data analysis
670 method testing the number of alleles in each gene with a phenotype against the number

671 of alleles in that gene without a mutant phenotype (Fisher's Exact Test) (Li *et al.* 2016,
672 2019; Fauser *et al.* 2022). Using this method, the authors hope to be confident that the
673 gene of interest is associated with a mutant phenotype in a given condition. However, in
674 doing so this method may exclude interesting genes that have many non-phenotypic
675 mutants due to insertions in 3'UTRs or introns, diluting the effect of strong alleles. In our
676 experimental setup, we enabled the use of variance-based statistical methods to identify
677 alleles with consistent heat-sensitive phenotypes. While single mutants showing a heat
678 sensitive phenotype cannot definitively prove a role of the disrupted genes in
679 thermotolerance, we think these data are valuable for several key reasons. (1) These
680 mutant phenotypes can be combined with other datasets such as multi-omics and
681 functional annotations to add validity to individual mutants; (2) strong phenotypes in
682 individual mutants can be used to guide the generation of additional mutants via other
683 mechanisms such as CRISPR (Picariello *et al.* 2020; Dhokane *et al.* 2020) to further
684 characterize the functions of interesting genes; and (3) these data may be used in the
685 future to characterize the specificity of gene x environment interactions by other groups.
686 Therefore, our triangulation approach comparing our HTGs with heat induced transcripts
687 and proteins and function annotations increased the confidence of our HTGs with roles in
688 thermotolerance.
689
690 We advanced the CLiP pooled screens under high temperatures in several ways.
691 Previous high temperature pooled mutant screens did not have a corresponding high
692 temperature transcriptome/proteome dataset for similar analyses (Fauser *et al.* 2022).
693 Additionally, our screens were performed in PBRs with well-controlled conditions to avoid
694 complicated effects due to nutrient deficiency and/or light shading, yielding reproducible
695 and consistent screen results. The heat treatments by Fauser et al. (2022) were provided
696 by heat blocks which were set at either 30°C or 35°C, without temperature probes inside
697 the algal cultures for temperature regulation. Thus, we suspect the actual temperature of
698 the algal cultures in the 2-L medium bottles they used may be lower than their targeted
699 high temperatures. In comparison, we grew the algal mutants in PBRs with precise
700 temperature regulation using sterile temperature probes inside each algal culture, so the
701 temperatures of our algal cultures were at or very close to our target temperatures.

702 Additionally, we included heat screens under 40°C which was absent from Fauser et al.
703 (2022) and they emphasized the mild high temperature of 30°C (Supplemental Dataset
704 1a). Thus, we identified more high confidence heat sensitive mutants (HSMs) than Fauser
705 et al. (2022). Finally, by requiring heat sensitive mutants to have normal growth rates
706 under the control condition of 25°C, we excluded genes that are essential under normal
707 growth conditions and only focused on genes with roles in thermotolerance.
708
709 Our 1,693 HTGs with high confidence HSMs overlapped with 10 of the 39 heat tolerance
710 genes (FDR < 0.3) and 2 of the 10 heat tolerance genes (FDR < 0.05) previously identified
711 by Fauser et al. (2022) (Supplemental Dataset 1i, j), validating our pooled screens.
712 Because both the treatment conditions and analysis pipelines were different between
713 Fauser et al. (2022) and ours, we would not expect perfect overlap between heat
714 tolerance genes identified. We identified three broad reasons why the remaining 29 genes
715 Fauser et al. (2022) identified were not included on our HTG list (Supplemental Dataset
716 1j): (1) due to differences in treatment conditions, some corresponding mutants had no
717 phenotypes in our pooled screen conditions, (2) some mutants had lower growth rates at
718 high temperatures than control, but didn't meet the stringent statistical cutoffs we
719 employed, or (3) some mutants had reduced growth rate (<0.95) at control conditions,
720 eliminating them in our analysis pipeline (we required normal growth rates at 25oC ≥
721 0.95). Nevertheless, we are confident that our methods built upon Fauser et al. (2022),
722 identified more high confidence HTGs (933 vs 39), and will advance our understanding
723 of thermotolerance in green algae.
724
725 **We identified genes with known roles in thermotolerance**
726 Our HTGs include genes with known roles in thermotolerance (Supplemental Dataset 1e),
727 further supporting the effectiveness of our screen conditions and analysis pipeline.
728 Among these genes were 26 chaperone proteins, which are involved in the proper folding
729 of proteins and are especially important under high temperatures (Schroda *et al.* 2015;
730 Rütgers *et al.* 2017). These include HSP22E HSP70A/H/C, and HSP90A. Additionally,
731 we identified 9 members of the Chlamydomonas carbon concentrating mechanism (CCM)
732 as HTGs. The CCM is responsible for increasing the CO_2 concentration near the Rubisco

733 active site, thereby increasing the rate of carbon fixation and decreasing the rate of
734 photorespiration, a costly process when Rubisco fixes O_2 rather than CO_2 (Mackinder
735 2018). The CCM is especially important under high temperatures, when the concentration
736 of dissolved CO_2 to O_2 decreases in liquid cultures (Blankenship 2014). Introducing the
737 CCM into plant cells has frequently been proposed to increase thermotolerance,
738 especially of C_3 plants (Mackinder 2018; Hennacy & Jonikas 2020). High temperature is
739 one of the driving forces for the evolution of CCM in C_4 plants in warm or tropical regions
740 (Sage 2004).
741
742 We identified both forms of Rubisco activase (RCA) as high confidence HTGs in
743 Chlamydomonas. RCA is responsible for removing sugar-phosphate inhibitory
744 compounds from the Rubisco catalytic site, which occurs with increased frequency under
745 high temperature and reduces Rubisco activity (Bhat, Thieulin-Pardo, Hartl & Hayer-Hartl
746 2017; Mueller-Cajar 2017). One of the primary limiting factors for carbon fixation during
747 high temperatures is the activation state of Rubisco (Crafts-Brandner & Salvucci 2002;
748 Perdomo, Capó-Bauçà, Carmo-Silva & Galmés 2017). Thermostable RCAs have been
749 frequently reported in plants grown in warm environments (Scafaro, Haynes & Atwell
750 1/2010; Shivhare & Mueller-Cajar 07/2017; Wang *et al.* 05/2010). Many plant species
751 express two RCA isoforms: the larger, redox regulated RCA-α and shorter RCA-β (Zhang
752 & Portis 1999; Bhat *et al.* 2017; Nagarajan & Gill 2018; Kim, Slattery & Ort 2020). In both
753 C_3 and C_4 plants, high temperature induces the transcript and protein level of RCA-α and
754 the rate of RCA-α induction is associated with the recovery rate of Rubisco activation and
755 photosynthesis (Kim *et al.* 2020; Anderson *et al.* 2021; Wang *et al.* 05/2010), suggesting
756 the important roles of RCAs in thermotolerance of photosynthesis under high
757 temperatures. Chlamydomonas has two copies of RCA, CrRCA1 and CrRCA2.
758 Chlamydomonas knockout mutants of CrRCA1 cannot grow well in air-level CO_2,
759 demonstrating its importance in photosynthesis (Pollock, Colombo, Prout, Godfrey &
760 Moroney 2003). The function of CrRCA2 is unknown. The CLiP CrRCA1 mutant have
761 insertions in 3' UTR, explaining it normal growth rate at the control 25°C with air and
762 supplied carbon. The protein sequence of CrRCA1 has higher similarity to the RCAs in
763 Arabidopsis than CrRCA2. CrRCA1 is the shorter RCA-β form, exhibiting redox regulation

764 despite lacking the regulatory C-terminal disulfide found in the RCA-α isoform of many
765 plant species (Pérez-Pérez *et al.* 2017; McConnell, Werth & Hicks 2018). At the transcript
766 level, *CrRCA1* is 30x more abundant than *CrRCA2* (Zhang *et al.* 2022). The transcripts
767 of both *CrRCA1/2* were induced during 40°C heat, and the protein of RCA1 was induced
768 during and after 40°C (Zhang *et al.* 2022), suggesting their important roles for heat
769 tolerance. Induced RCAs may help maintain photosynthesis under high temperatures,
770 alleviating over-reduced photosynthetic electron transport chains.
771
772 **We identified core heat tolerance genes among different heat treatments**
773 We found 56 HTGs with heat sensitive mutants in all of our four conditions, representing
774 the list of core heat tolerance genes (Supplemental Dataset 1g). Fifteen of these genes
775 had no annotations, representing novel putative HTGs of great interest for future
776 characterization. *CrRCA1* was again present in this gene set, highlighting its importance
777 in thermotolerance. Additionally, this gene set contained the PSII assembly/repair factor
778 HCF136. In Arabidopsis, HCF136 is required for the proper insertion of the core reaction
779 center protein, D1, into the PSII complex (Plöchinger, Schwenkert, von Sydow, Schröder
780 & Meurer 2016). High temperatures reduce photosynthesis, increase ROS production,
781 and lead to oxidative stress. The D1 protein is frequently damaged during oxidative stress
782 conditions, resulting in its removal and insertion of a new D1 protein into the reaction
783 center (Järvi, Suorsa & Aro 2015; Theis & Schroda 2016). Without the HCF136 protein,
784 these mutants likely cannot cope with the oxidative stresses caused by high temperatures
785 and perform poorly in pooled screens with heat treatments.
786
787 Additionally, the list of core HTGs contained several putative signal transduction pathway
788 members, including three adenylate/guanylate cyclases and three 3'-5' cyclic nucleotide
789 phosphodiesterases (Supplemental Dataset 1g). While previous reports have shown that
790 both unfolded proteins (Rütgers *et al.* 2017) and calcium spikes (Königshofer, Tromballa
791 & Löppert 2008; Saidi *et al.* 2009; Wu, Luo, Vignols & Jinn 2012) can lead to the activation
792 of heat shock transcription factors to induce the heat stress response(Schulz-Raffelt,
793 Lodha & Schroda 2007; Schmollinger, Strenkert & Schroda 2010; Schroda *et al.* 2015),

794 the signaling cascades leading to these responses remain unknown. These six genes are
795 prime candidates for putative members of these signaling cascades.
796
797 **HTGs are overrepresented in the secretory pathway**
798 We found that HTGs are overrepresented for proteins localizing to the secretory pathway
799 (Figure 4d). Secretomes are known to contain proteins with a variety of functions including
800 cell wall maintenance, redox homeostasis, and cell-cell communication (Krause, Richter,
801 Knöll & Jürgens 2013; Tanveer, Shaheen, Parveen, Kazi & Ahmad 2014). Recent works
802 across a range of plant species have shown that secretomes vary widely in response to
803 different environmental stresses, including oxidative (Zhou, Bokhari, Dong & Liu 2011;
804 Tanveer *et al.* 2014), drought (Pandey *et al.* 2010; Bhushan *et al.* 2011; Krause *et al.*
805 2013; Tanveer *et al.* 2014), osmotic (Zhang *et al.* 2009; Song *et al.* 2011; Tanveer *et al.*
806 2014; Ngara *et al.* 2018), and low temperature stresses (Gupta & Deswal 2012; Tanveer
807 *et al.* 2014). Furthermore, a recent analysis in Chlamydomonas comparing an evolved
808 salinity-tolerant strain to the parental strain found over 500 differentially expressed
809 proteins between the two secretomes (Ves-Urai, Krobthong, Thongsuk, Roytrakul &
810 Yokthongwattana 2021). Recently, a high temperature secretome of *Sorghum bicolor* cell
811 cultures identified 31 heat-responsive secreted proteins functioning in protein
812 modification, detoxification, and metabolism (Ngcala, Goche, Brown, Chivasa & Ngara
813 2020). Though the Chlamydomonas secretome under high temperatures has not yet been
814 explored, we hypothesize that some of HTGs in the secretory pathway may enhance the
815 thermotolerance of Chlamydomonas cells.
816
817 **Carbon availability affects the thermotolerance of green algae**
818 The WT background of the CLiP library, CC-5325, exhibits different growth rates at
819 moderate and acute high temperatures of 35°C and 40°C depending on carbon availability
820 (Figure 1a). Heat at 30°C and 35°C increased the growth of CC-5325 with supplied carbon
821 (TAP medium), but this increase was abolished without supplied carbon (TP medium).
822 These observations led us to hypothesize that the presence of external carbon improves
823 the thermotolerance of Chlamydomonas, at least for 2 days in our heat experiments. To
824 understand the molecular mechanisms underpinning this observation, we investigated

825 the functional enrichment of HTGs identified from both the TAP-35°C and TAP-40°C
826 conditions. We found that genes involved in glycolysis, particularly pyruvate kinases, were
827 significantly enriched in this gene set and unique to screen conditions with supplied
828 carbon source (Figure 5b). Glycolysis is an important part of the central carbon
829 metabolism and plays a key role in the breakdown of starch for utilization as cellular
830 energy (Johnson & Alric 2012, 2013). Pyruvate kinase catalyzes the final step of
831 glycolysis, which converts phosphoenolpyruvate and one ADP to pyruvate and one ATP
832 (Baud *et al.* 2007; Wulfert, Schilasky & Krueger 2020). Three pyruvate kinases were
833 identified in these significantly enriched MapMan terms: PYK3 (Cre05.g234700), PYK4
834 (Cre03.g144847), and PYK6 (Cre10.g426292). In plant systems, there are commonly
835 multiple pyruvate kinase isoforms localizing to either the plastid or the cytosol (Plaxton
836 1996; van Dongen *et al.* 2011). The carbon source, acetate, present in the TAP medium
837 is up-taken through the acetate uptake/assimilation pathway then converted to starch via
838 the glyoxylate and gluconeogenesis cycles in Chlamydomonas (Johnson & Alric 2012,
839 2013). Indeed, our previous work in WT Chlamydomonas cells showed that most proteins
840 involved in acetate uptake/assimilation and glyoxylate and gluconeogenesis cycles were
841 induced during 35°C heat and starch content increased in 35°C treated cells in TAP
842 medium (Zhang *et al.* 2022). Increased starch breakdown through the glycolysis cycle
843 and production of cellular energy is likely contributing to the enhanced thermotolerance
844 and growth rates of Chlamydomonas in acetate-supplied conditions. The three copies of
845 PYK with heat sensitive mutants in TAP medium may be important for catalyzing the
846 breakdown of phosphoenolpyruvate and production of ATP under high temperatures.
847 Under other stress conditions, for example low oxygen, allosteric regulation leads to
848 increased activity of PYKs resulting in greater ATP production (van Dongen *et al.* 2011).
849 While the majority of respiratory ATP production typically comes from oxidative
850 phosphorylation in mitochondria, the ATP production from glycolysis can be important
851 under stressful conditions where energy availability is limited (van Dongen *et al.* 2011). A
852 recent proteomics analysis in barley under heat stress also found that utilization of
853 glycolysis as an alternative energy source is important for thermotolerance (Rollins *et al.*
854 2013). The normal growth phenotypes of the *pky* mutants under control conditions may
855 be explained either by functional redundancy (Chlamydomonas has 6 PYKs), or by

856 stress-specific need for higher enzyme function to increase the production of ATP for use
857 in production of HSPs, maintenance of RCA activity, increased ion channel activities, and
858 other cellular processes under high temperatures.
859
860 In comparison to the TAP conditions, there was little functional enrichment for the HTGs
861 in both TP conditions apart from the flagellar radial spoke head, which has a putative role
862 in mechanoregulation of ciliary beating (Grossman-Haham *et al.* 2021). This may be
863 partially explained by the overall smaller overlap between HTGs in both TP conditions as
864 compared to both TAP conditions. While there were 700 (56+83+160+401, No. above
865 vertical bars, Figure 5a) HTGs found in both TAP conditions, representing 42% of the
866 35°C and 36% of the 40°C HTGs, there were only 159 (56+23+32+48) HTGs found in
867 both TP conditions, representing just 15% of 35°C and 17% of 40°C HTGs. This may be
868 due to the slower growth rates (thus fewer generations) in TP conditions without organic
869 carbon source. This may also reflect a more diverse set of genes required for tolerance
870 of different high temperatures in the absence of external carbon sources. Future work
871 expanding the length of the screen in TP conditions, thereby increasing the number of
872 generations in the screen, may improve the resolution of HTGs during high temperatures
873 without organic carbon source.
874
875 **Different high temperature treatments result in some non-overlapping HTGs**
876 Next, by comparing the functional enrichment of HTGs in both 35°C treatments to those
877 in both 40°C treatments, we identified functional categories that are differentially required
878 under the different heat treatments. Unlike the comparison between TAP and TP
879 conditions, there were a similar number of HTGs identified in each temperature treatment,
880 with 428 (56+23+160+189) HTGs found in both 35°C conditions and 343 HTGs
881 (56+32+83+172) found in both 40°C conditions (Figure 5a). Within the overlapping 35°C
882 HTGs, calcium signaling was significantly enriched (Figure 5b). Calcium signaling
883 pathways have been frequently implicated in thermotolerance in photosynthetic cells,
884 however the members involved in this pathway are not well understood (Königshofer *et*
885 *al.* 2008; Saidi *et al.* 2009; Wu *et al.* 2012). Of the 62 genes with annotated roles in calcium
886 signaling represented in this screen, 8 have heat sensitive mutants in both TAP-35°C and

887 TP-35°C conditions (Figure 5b, Supplemental dataset 3d**)**. These included four putative
888 calmodulin-dependent protein kinases, two putative ATPases, one putative copine
889 protein (Tomsig & Creutz 2002), and one protein with an annotated calmodulin domain
890 but no other known functions. These genes provide novel insight into the putative calcium
891 signaling pathways that are important for the thermotolerance of photosynthetic cells. Of
892 particular interest is FAP39 (Cre02.g145100), a putative cation transporting ATPase
893 localized to the flagella. Some researchers have hypothesized that a heat sensor may be
894 flagellar localized or related to flagellar function in green algae and other organisms
895 (Kamp & Higgins 2011; Sengupta & Garrity 2013; Sekiguchi, Kameda, Kurosawa,
896 Yoshida & Yoshimura 2018), but the mechanisms remain unknown. Furthermore, we
897 identified several cell motility MapMan terms significantly enriched in the 35°C HTGs.
898
899 The 40°C HTGs were significantly enriched for calcineurin (CaN) like phosphoesterases.
900 Of the three CaN-like phosphoesterases in this screen, two were identified as HTGs in
901 the 40°C condition (Figure 5b). These calmodulin-dependent serine/threonine
902 phosphoesterases do not have clearly defined roles in Chlamydomonas, but we
903 hypothesize that they are involved in thermotolerance-related signaling pathways. It is
904 possible that these proteins are somehow involved in distinguishing between different
905 intensities of temperature stresses, but the mechanisms of this are unclear. Future work
906 to identify the molecular function of these proteins could provide novel insight into the
907 signaling pathways involved in thermotolerance.
908
909 **Our research can be used to improve thermotolerance in land plants**
910 To translate our algal research to land plants, we identified orthologs of high confidence
911 HTGs in key land plants of interest (Figure 8) and about 50% of them are highly conserved
912 in land plants, suggesting we can study the function of these HTGs in Chlamydomonas
913 to infer the function of these genes in land plants. We highlighted the functionality of our
914 study in Chlamydomonas by testing the heat sensitivity of Arabidopsis mutants deficient
915 in the *AtHMT* gene, which is ortholog to a high confidence Chlamydomonas HTG. The
916 Arabidopsis mutant *hmt-2* displayed significantly reduced plant size as compared to WT
917 following heat treatments, demonstrating the translatability of our work in

Chlamydomonas to land plants. Histone post-translational modifications alter nucleosome properties, affect chromatin structure and its interactions with other proteins, and impact gene regulation (Crisp, Ganguly, Eichten, Borevitz & Pogson 2016; Ueda & Seki 2020). Histone methylation can either increase or decrease transcription, depending on the amino acid position of the methylation and the number of methyl groups attached to specific histone tails. In Arabidopsis, H3K4me3 (trimethylation of histone H3 at lysine 4) is associated with actively transcribed genes while H3K27me3 is often associated with lowly expressed genes (Oberkofler, Pratx & Bäurle 2021; Friedrich *et al.* 2021; Hu & Du 2022). The *AtHMT* gene is annotated as histone-lysine N-methyltransferase, although its detailed function is unknown. We hypothesize that the epigenetic modifications performed by *AtHMT* and *CrHMT* are required for the regulation of heat responses in photosynthetic cells, which needs function validation in the future.

Chlamydomonas is not only a powerful model organism for production of algal biofuels and bioproducts, but also an excellent model for the study of thermotolerance in photosynthetic cells. Our research in Chlamydomonas advances understanding of heat response in photosynthetic cells and identifies important engineering targets to improve thermotolerance in both algae and crops.

Acknowledgements

This research was supported by start-up funding from the Donald Danforth Plant Science Center (DDPSC), and sequencing service support from the Department of Energy (DOE) Joint Genome Institute (JGI) Community Science Program (CSP, 503414), and the DOE Biological & Environmental Research (BER) grant (DE-SC0020400) to R.Z. The work (proposal: 10.46936/10.25585/60001126) conducted by the U.S. Department of Energy Joint Genome Institute (https://ror.org/04xm1d337), a DOE Office of Science User Facility, is supported by the Office of Science of the U.S. Department of Energy operated under Contract No. DE-AC02-05CH11231. E.M.M. is supported by the William H. Danforth Plant Sciences Fellowship, DDPSC startup funding to R.Z. and Washington University in St. Louis. J.C. and C. C. was supported by DOE grant (DE-SC0020400) and NIH grant (R01GM093123). J.E was partially supported by the National Science

948 Foundation (NSF) Research Experience for Undergraduates (REU) program at DDPSC,
949 NSF grant DBI-1659812. We are grateful for Dr. Martin Jonikas for using the CLiP mutant
950 library for our pooled screens. We would like to thank Dr. Friedrich Fauser, Dr. Xiaobo Li,
951 Dr. Robert Jinkerson, and Weronika Patena for discussion about the CLiP mutant library,
952 Jeff Berry for helpful suggestions for statistical analyses, Maria Sorkin and Natasha Bilkey
953 for advice regarding experiments in Arabidopsis, Dr. Dan Lin for donation of wild type Col-
954 0 Arabidopsis seeds, Drs. Saima Sahid, Kaushik Panda, and Benedikt Venn for their
955 helpful suggestions regarding functional enrichment analyses, Riya Patel for helping with
956 photobioreactor maintenance and sample harvesting, Luisa Galhardo for helping with
957 medium preparation, and Margarita Ramirez for her preliminary analysis of comparing
958 novel heat tolerance genes with previously published RNA-seq data.

959 **Author Contributions**

960 R.Z. supervised the whole project, conducted pooled mutant screens in photobioreactors
961 and collected cell samples. E.M.M., W.M., and N.Z. prepared samples for barcode
962 extraction and sequencing. DOE JGI CSP team (C.G.D., M. Z., C.P., J.S., R.C.O.),
963 sequenced the DNA barcodes. E.M.M and W.M. developed data analysis pipeline for
964 identification of heat sensitive mutants. E.M.M. led the project with data analysis, and
965 figure preparation. C.E.B., W.M., and N.Z. completed growth rate validation of individual
966 mutants in monocultures. J.E., E.M.M., and C.E.B. verified the identity of individual
967 mutants used for monoculture phenotyping. C.C. and J.C. completed analysis of genes
968 with ChlamyNet database. E.M.M. performed heat sensitivity assay in Arabidopsis
969 mutants. E.M.M. and R.Z. led the writing of the manuscript. C.E.B. and C.C. wrote their
970 corresponding methods. R.Z., E.M.M., J.E., C.E.B., J.C. and C.C. helped edit the
971 manuscript.

972 **Main text figure legends**

973 **Figure 1: We screened the CLiP Chlamydomonas mutant library under either 35ºC**
974 **or 40ºC with and without supplied carbon source using quantitative pooled**
975 **screens. (a)** The relative growth rates of Chlamydomonas wildtype cells (CC-5325, CLiP
976 library background strain) at different temperatures with and without supplied carbon

977 source. Chlamydomonas cells were grown in photobioreactors (PBRs) in Tris-acetate-
978 phosphate (TAP, with acetate, a carbon source) or Tris-phosphate (TP, no acetate)
979 medium under turbidostatic conditions at different temperatures with a light intensity of
980 100 μmol photons m^{-2} s^{-1} and constantly bubbling of air. Relative growth rates were
981 calculated based on the cycling of OD_{680}, which is proportional to total chlorophyll content
982 in unit of μg chlorophyll mL^{-1}. Each temperature treatment was conducted in an individual
983 PBR and lasted two days. Mean ± SD, n = 2-5 biological replicates. Statistical analyses
984 were performed using two-tailed t-test assuming unequal variance by comparing with
985 25°C with the same carbon condition (*, $p < 0.05$, the color and position of asterisks match
986 the treatment conditions). **(b)** Pooled CLiP mutants were grown in PBRs with either TAP
987 or TP medium under different temperature treatments with turbidostatic conditions.
988 Cultures were acclimated for 2 days at 25°C under 100 μmol photons m^{-2} s^{-1} light before
989 high temperature treatments. Heat at 35°C (brown lines) lasted for 4 days (TAP) or 5 days
990 (TP). Heat at 40°C lasted for 2 days then recovered at 25°C for 3 days (red) for both TAP
991 and TP conditions. Algal cultures grown at 40°C for longer than two days could not
992 survive. Control cultures were maintained at 25°C for the duration of the experiment (dark
993 blue). Different treatments were conducted in individual PBRs. Samples were collected
994 at the beginning (T1) and the end (T3a or T3b) of the treatment period. T3a or T3b marked
995 the end of the screens, but T3a was one day shorter than T3b. T3a was used for the end
996 of TAP-35°C screen, while T3b was used for all other screens due to their slower growth
997 rates than TAP-35°C. **(c)** Schematic of pooled screens utilizing unique internal DNA
998 barcodes of the CLiP mutant library. The Chlamydomonas CLiP mutant library enables
999 high-throughput, quantitative phenotyping in pooled cultures. Three hypothetical mutants
1000 are shown, each with a unique DNA barcode sequence (represented by purple, brown,
1001 and red bars). CLiP mutants are pooled and grown under the condition as in panel b.
1002 Under constant 25°C, three mutants have no change of growth rates, thus no change of
1003 barcode abundance. If the brown (or red) mutant is deficient in a process essential for
1004 optimal growth under a 35°C (or 40°C) screen condition, it will have reduced cell
1005 abundance at the end of the screen. Algal cells are harvested at the start and end of the
1006 screen for DNA extraction and barcode amplification. Cell abundance and growth rate of
1007 each mutant in pooled cultures are calculated by quantifying DNA barcodes using deep

1008 sequencing from pooled mutant DNAs. **(d)** Principal component (PC) analysis of
1009 normalized barcode abundance from each sample. The first two PC displayed represent
1010 the largest amount of variance explained in the dataset. Closed symbols and solid ovals
1011 represent TAP conditions, open symbols and dashed ovals represent TP conditions.
1012 Colors represent the different temperature treatment groups (blue: 25°C; brown: 35°C;
1013 red: 40°C) and shapes represent sampling time points (T1, T3a, T3b). PVE: percent
1014 variance explained.
1015
1016 **Figure 2: Growth rates calculated from barcode quantification are reproducible. (a,**
1017 **b)** Growth rates of one mutant with two different barcodes were consistent. Some mutants
1018 have two different barcodes (from 5' and 3' side of the insertional cassette or from 2
1019 different insertion sites). Different barcodes from the same mutants were amplified and
1020 sequenced separately. Each dot represents one mutant with two different barcodes. X-
1021 and Y-axes are mean normalized growth rates calculated from two different barcodes of
1022 the same mutant in the screens of TAP-25°C (a) and TAP-35°C (b). r: Pearson correlation
1023 coefficient. **(c, d)** Growth rates of biological replicates can be calculated consistently.
1024 Each dot represents the normalized growth rate of one mutant from two biological
1025 replicates in the screens of TAP-25°C (c) and TAP-35°C (d). Because the screen pressure
1026 was present under TAP-35°C but not TAP-25°C, the growth rate plots from the two
1027 conditions are different. **(e)** Growth rates calculated from pooled mutant screens were
1028 validated with those calculated from monocultures for 10 individual CLiP mutants. X:
1029 mean relative growth rates of individual CLiP mutants from TAP-25°C (black) or TAP-
1030 35°C (brown) calculated from pooled mutant screens. Y: relative growth rates of individual
1031 CLiP mutants calculated from monoculture growth experiments normalized to WT CC-
1032 5325 under the same condition. The identity of mutants used for monocultures were
1033 validated by PCR. For monoculture experiments, individual CLiP mutants were grown in
1034 PBRs as mentioned in Figure 1b, like the pooled screens. Two or three bio-replicates
1035 were conducted for most of the CLiP mutants (see mutant IDs and No. of replicates in
1036 Supplemental Dataset 1b). Mutants that were depleted in the heat screens were set to
1037 have a growth rate of zero in the pooled screens for the plot.
1038

1039 **Figure 3: Heat-compromised and heat-depleted mutants were identified from**
1040 **quantitative pooled screens. (a-d)** Heat-compromised (comp-) mutants from TAP-35°C
1041 (**a**), TP-35°C (**b**), TAP-40°C (**c**), TP-40°C (**d**) were defined as those with mean normalized
1042 growth rates at 25°C ≥ 0.95, mean normalized growth rates at 35°C or 40°C ≤ 0.8, p-value
1043 < 0.05 and t-values in the 95th percentile (student's one-sided t-test of unequal variance,
1044 red dots). Heat-depleted individuals were defined as those that were absent from the
1045 35°C or 40°C pools at the end of the screen but had normal growth at 25°C (≥0.95),
1046 indicated in the bottom right corner of each panel.
1047
1048 **Figure 4: Heat sensitive mutants disrupted in putative heat tolerance genes (HTGs)**
1049 **were characterized at the genome-wide level.** Each CLiP mutant has a mapped
1050 insertion site, thus a mapped disrupted gene. We identified putative HTGs from heat
1051 sensitive mutants (HSMs). **(a)** Distribution of insertion features from HSMs (purple) is
1052 similar to that from the CLiP library screened (gray). Insertion feature refers to the
1053 integration sites of the transforming cassette relative to gene components, e.g.,
1054 untranslated regions (UTRs), coding sequence (CDS), or introns. **(b**) Distribution of
1055 confidence levels from HSMs (orange) is similar to that from the CLiP library screened
1056 (gray). Insertion confidence refers the likelihood of the mapped insertion sites being
1057 correctly identified based on genomic sequences flanking the insertional cassette, with
1058 levels 1 and 2 for the highest confidence (95%) of the mapped insertion sites, level 3 for
1059 73% confidence, level 4 for 58% confidence. **(c)** For HTGs identified from each of the four
1060 treatment conditions, the number of alleles that were significantly heat sensitive are
1061 shown. Green, orange, and purple bars represent 1, 2, or ≥ 3 heat sensitive alleles,
1062 respectively. **(d)** HTGs identified in any of the four treatment conditions were aggregated
1063 and the distribution of predicted subcellular localizations is displayed. Significant
1064 enrichment for the secretory pathway was found (*, Fisher's exact test, p < 0.01).
1065 Percentage shown of each localization is the % of HTGs with this predicted subcellular
1066 localization out of all HTGs identified with a predicted subcellular localization.
1067
1068 **Figure 5: Heat tolerance genes (HTGs) were overlapped between conditions for**
1069 **functional enrichment. (a)** HTGs overlap between conditions. From the identified heat

1070 sensitive mutants, we generated a list of genes with potential roles in heat tolerance,
1071 defined as HTGs, which are those with at least 1 heat-compromised or heat-depleted
1072 mutant in a screen condition under high temperatures. To compare between conditions,
1073 only genes represented by at least one mutant in all four conditions were included in this
1074 analysis. Horizontal bars represent the total number of HTGs from each condition. Vertical
1075 bars and the number on their top represent the number of genes included in each overlap.
1076 Circles along x-axis represent the conditions included in each overlap in the vertical bars.
1077 Filled circles represent TAP conditions and open circles represent TP conditions; circle
1078 colors represent the temperature of heat treatments, brown for 35°C and red for 40°C.
1079 Genes belong to only a single intersection category and are sorted into the category with
1080 the greatest number of intersections. (**b**) MapMan functional enrichment of all HTGs
1081 identified (those with at least one heat sensitive mutant in at least one condition), both
1082 TAP conditions, both TP conditions, both 35°C conditions, both 40°C conditions, and all
1083 4 conditions are shown. Only significantly enriched MapMan terms are shown (FDR <
1084 0.05). Size of each circle indicates the number of HTGs in a given MapMan term. Color
1085 of the circles represent the FDR adjusted p-value. Numbers in parentheses after each
1086 Mapman term is the total number of genes assigned to the given MapMan term and
1087 present in the pooled screen dataset.
1088
1089 **Figure 6: Comparison of heat tolerance genes (HTGs) with transcriptome and**
1090 **proteome data under high temperature. (a, b)** Venn diagrams comparing HTGs with
1091 heat induced genes/proteins (HIGs/HIPs) from 35°C and 40°C treatments of WT cultures
1092 in TAP medium (Zhang *et al.* 2022). Exp, expected overlapping numbers based on
1093 random chance. *, $p < 0.05$, Fisher's Exact Test based on the indicated background size.
1094 **(c)** Select weighted correlation network analysis (WGCNA) modules that were
1095 overrepresented for HTGs above random chance (*, $p < 0.05$, Fisher's exact test). TM:
1096 transcriptomic module. Consensus transcription patterns from TAP-40°C (red) and TAP-
1097 35°C (brown) are shown. Numbers at the top of each module display: the total number
1098 (No.) of genes in the given module that were represented by at least one mutant in the
1099 pooled screens (before /, black) and the total No. of aggregated HTGs in that module
1100 from all four treatment conditions (after /, blue). Numbers at the right of each plot show

1101 the No. of HTGs from TAP-40°C (red, top) and TAP-35°C (brown, bottom), respectively.
1102 Functional enrichment on right side of each module shows select significantly enriched
1103 MapMan terms from TAP-40°C HTGs (top, red), TAP-35°C HTGs (middle, brown) and
1104 the aggregated list of HTGs from all four conditions (bottom, blue) that are present in a
1105 given module (FDR < 0.05).
1106
1107 **Figure 7: A triangulation approach was used to identify high confidence heat**
1108 **tolerance genes (HTGs**). (**a**) High confidence HTGs were defined using a triangulation
1109 approach based on three criteria: (A): HTGs in our pooled screens that had at least one
1110 heat sensitive mutant (HSMs) in at least two conditions or at least two heat sensitive
1111 mutant alleles in any one condition (defined as high confidence HSMs); (B): heat inducible
1112 during the high temperature treatment of previously published RNA-seq or proteomic
1113 data; (C): MapMan functional annotation in select categories that may be involved in
1114 thermotolerance or affected by high temperatures. MapMan functional categories
1115 included in this analysis are displayed in cartoon on the right. Genes that meet at least
1116 two of these three criteria were considered as high confidence HTGs. The number of
1117 genes overlapping between any two categories are displayed next to arrows connecting
1118 criteria. Of the 504 genes overlapping between criteria A and B, 282 had no MapMan
1119 functional annotations (U) and 222 had at least one MapMan functional annotation (K).
1120 Of the 222 genes with functional annotations, functional enrichment analysis with
1121 abbreviated MapMan terms is displayed (right). Size of each circle indicates the number
1122 of overlapping HTGs in a given MapMan term. Color of the circles represent the adjusted
1123 p-value. For full list of MapMan annotations included in this analysis see Supplemental
1124 Dataset 3j. (**b**) Visualization of high confidence HTGs in the transcription network topology
1125 of ChlamyNET, a web-based network tool that was generated based on published
1126 transcriptomes in Chlamydomonas (Romero-Campero *et al.* 2016). Nine gene clusters
1127 with different function enrichment were identified by ChlamyNET, represented by different
1128 colors. Each dot represents one Chlamydomonas gene in the network. The genes circled
1129 in black are the high confidence HTGs. Of the 933 high confidence HTGs, 594 were
1130 present in the ChlamyNET network of 9,171 genes. Stars (*) indicate significant
1131 enrichment for high confidence HTGs within the three ChlamyNet clusters (FDR < 0.05).

1132 The overrepresentation analysis and scatterplot visualization are performed using the R
1133 programming language.
1134
1135 **Figure 8: Many Chlamydomonas high confidence heat tolerance genes (HTGs) are**
1136 **conserved throughout the green lineage. (a)** Chlamydomonas high confidence HTGs
1137 were classified by their orthology to *Volvox carterii* (Volvox), *Arabidopsis thaliana*
1138 (Arabidopsis), *Oryza sativa* (Rice), *Triticum aestivum* (wheat), *Glycine max* (Soybean),
1139 *Zea mays* (Maize), *Sorghum bicolor* (Sorghum), and *Setaria viridis* (Setaria) genes using
1140 the InParanoid ortholog dataset. **(b)** Mean transcript per million (TPM) normalized read
1141 counts of the Chlamydomonas putative histone-lysine N-methyltransferase (HMT) gene
1142 during and after high temperatures of 35ºC (brown curve) or 40ºC (red curve) (modified
1143 from Zhang et. al., 2022). Mean ± SD, *n*=3. Stars indicate significance in differential
1144 expression modeling. (**c, d**) Three CLiP alleles of *CrHMT* were heat sensitive in our
1145 pooled mutant screens. Stars indicate significance in pooled screen data. Mean ± SD,
1146 *n*=2. (e) Two mutant alleles of Arabidopsis AtHMT (one-to-one ortholog), *Athmt-1* and
1147 *Athmt-2* were used for phenotype verification in land plants. (**f**) Representative plate
1148 images of 14-day old seedlings from control (25ºC) and treatment (41ºC for 45 minutes
1149 followed by 7 days of recovery at 25ºC). (**g**) Mean plantlet area relative to wild type (Col-
1150 0) of *hmt-1*, *hmt*-2, and *hot1* (positive control, a well-characterized heat sensitive mutant,
1151 deficient in Heat Shock Protein HSP101). Plantlet area was quantified using ImageJ and
1152 normalized to the total area of Col-0 on the same plate. Mean ± SD, *n*=3. *, $p < 0.05$,
1153 student's one-sided t-test of unequal variance.
1154
1155 **Supplemental Figure Legends**
1156
1157 **Figure S1: Normalized read counts of biological replicates are highly reproducible.**
1158 Normalized reads for each barcode in two biological replicates are shown for every
1159 condition and time point. Linear model of best fit shown in red line. Pearson correlation
1160 coefficient are displayed. Treatment groups are displayed in columns (25ºC, 35ºC, and
1161 40ºC from left to right). Time points are displayed in rows (T1, T3a, T3b from top to bottom.

1162 **(a)** All TAP (Tris-acetate-phosphate medium) conditions with supplied carbon source. **(b)**
1163 All TP (Tris-phosphate medium) conditions without supplied carbon source.
1164
1165 **Figure S2: We used statistical cutoffs to identify heat sensitive mutants**. Heat
1166 sensitive mutants are required to have normal growth rates at 25ºC (≥ 0.95) and reduced
1167 mean normalized growth rates at 35ºC or 40ºC (≤ 0.8), p-value < 0.05, and t-values in the
1168 95th percentile (student's one-sided t-test of unequal variance). **(a-f)** Distribution of mean
1169 growth rates of all mutants in each condition. Dashed lines represent growth rates cutoffs.
1170 Growth rate cutoff values are displayed at the start of the arrows. Percentage under the
1171 arrows quantifies the fraction of barcodes that meet the growth rate cutoffs. **(g-j)** Empirical
1172 distributions of t-values for all tests per condition. T-values are based on both the
1173 difference between means and the variance between biological replicates. Vertical
1174 dashed lines display the 95th percentile mark for each empirical distribution. Numbers
1175 above the arrows display the cutoff t-values. Only the top 5% of t-values were considered
1176 statistically significant, in addition to p-values < 0.05.
1177
1178 **Figure S3: Some heat tolerance genes (HTGs) may be also involved in other**
1179 **stresses.** The 1,693 heat tolerance genes (HTGs) with high confidence heat sensitive
1180 mutants (HSMs) identified in our screens were compared with previously published
1181 screen data (Fauser et al. 2022) from approximately 121 pooled screen conditions, sorted
1182 into 16 broad categories with FDR<0.3. These 1693 HTGs refer to those that have at
1183 least one HSM in at least two conditions or at least two HSM alleles in any one condition
1184 in our pooled screens. Bars quantify the % of overlapping HTGs with sensitive mutants in
1185 the given condition (numerator) out of all genes with sensitive mutants in that condition
1186 (denominator). Numbers after horizontal bars are No. of genes with significantly sensitive
1187 mutants in that condition and also overlap with our HTGs (before /) and No. of genes with
1188 significantly sensitive mutants in that condition (after /). The ratios of these two numbers
1189 are the % presented by the X axis.
1190
1191 **Supplemental Dataset 1: (a)** Overview of screen conditions used in this publication and
1192 previous pooled screens by Fauser et al. (2022). **(b)** List of primers used in this

publication. **(c)** Number of generations per biological replicate used to calculate growth rates of mutants in pooled cultures. **(d)** Identification of heat tolerance genes (HTGs) with heat-compromised and heat-depleted mutants in each of all four conditions. **(e)** HTGs with known thermotolerance roles. **(f)** HTGs that are putative transcription factors according to the Plant Transcription Factor Database. **(g)** Core HTGs: HTGs with heat sensitive mutants in all four conditions. **(h)** List of 1,690 HTGs with high confidence heat sensitive mutants. (**i**) Number of genes from the high temperature screens of Fauser et al. (2022) that were identified as HTGs with high confidence heat sensitive mutants in this study. **(j)** Phenotype of HTGs from Fauser et al. (2022) in this study. **(k)** Genes in transcriptional modules 1 and 3 from Zhang, et. al. 2022 that are also HTGs in this study. **(l)** All HTGs that meet triangulation cutoffs (at least 2 of 3 criteria). **(m)** HTGs that meet all three triangulation criteria. **(n)** One-to-one orthologs of high-confidence HTGs in Arabidopsis.

Supplemental Dataset 2: All pooled screen data calculated from every barcode represented in pooled mutant screens presented in this publication.

Supplemental Dataset 3: MapMan functional enrichment outputs for all analyses presented in this publication. MapMan functional enrichment for HTGs that are present in: (**a**) at least one heat screen conditions; (**b**) both TAP-35°C and TAP-40°C; (**c**) both TP-35°C and TP-40°C; (**d**) both TAP-35°C and TP-35°C; (**e**) both TAP-40°C and TP-40°C; (**f**) all four heat screen conditions; (**g**) TM1; (**h**) TM3; (**i**) triangulation criteria A and B. (**j**) List of MapMan terms used to generate criterion C of the triangulation approach.

References

Alonso J.M., Stepanova A.N., Leisse T.J., Kim C.J., Chen H., Shinn P., … Ecker J.R. (2003) Genome-wide insertional mutagenesis of *Arabidopsis thaliana*. *Science* **301**, 653–657.

Anderson C.M., Mattoon E.M., Zhang N., Becker E., McHargue W., Yang J., … Zhang R. (2021) High light and temperature reduce photosynthetic efficiency through

1225 different mechanisms in the C_4 model Setaria viridis. *Communications Biology* **4**,
1226 1092.
1227 Balfagón D., Sengupta S., Gómez-Cadenas A., Fritschi F.B., Azad R.K., Mittler R. &
1228 Zandalinas S.I. (2019) Jasmonic acid Is required for plant acclimation to a
1229 combination of high light and heat stress | Plant Physiology. *Plant physiology* **181**,
1230 1668–1682.
1231 Baud S., Wuillème S., Dubreucq B., de Almeida A., Vuagnat C., Lepiniec L., … Rochat
1232 C. (2007) Function of plastidial pyruvate kinases in seeds of *Arabidopsis thaliana*.
1233 *The Plant journal: for cell and molecular biology* **52**, 405–419.
1234 Benjamini Y. & Hochberg Y. (1995) Controlling the false discovery rate: a practical and
1235 powerful approach to multiple testing. *Journal of the Royal Statistical Society.*
1236 *Series B, Statistical methodology* **57**, 289–300.
1237 Bhat J.Y., Thieulin-Pardo G., Hartl F.U. & Hayer-Hartl M. (2017) Rubisco Activases: AAA+
1238 Chaperones Adapted to Enzyme Repair. *Frontiers in molecular biosciences* **4**, 20.
1239 Bhushan D., Jaiswal D.K., Ray D., Basu D., Datta A., Chakraborty S. & Chakraborty N.
1240 (2011) Dehydration-responsive reversible and irreversible changes in the
1241 extracellular matrix: comparative proteomics of chickpea genotypes with
1242 contrasting tolerance. *Journal of proteome research* **10**, 2027–2046.
1243 Blankenship R.E. (2014) *Molecular Mechanisms of Photosynthesis, Second Edition*.
1244 Wiley Blackwell, John Wiley & Sons, Ltd, The Atrium, Southern Gate, Chichester,
1245 West Sussex, PO19 8SQ, UK.
1246 Cha J.-Y., Kang S.-H., Ali I., Lee S.C., Ji M.G., Jeong S.Y., … Kim W.-Y. (2020) Humic
1247 acid enhances heat stress tolerance via transcriptional activation of Heat-Shock
1248 Proteins in Arabidopsis. *Scientific reports* **10**, 15042.
1249 Conway J.R., Lex A. & Gehlenborg N. (2017) UpSetR: an R package for the visualization
1250 of intersecting sets and their properties. *Bioinformatics* **33**, 2938–2940.
1251 Crafts-Brandner S.J. & Salvucci M.E. (2002) Sensitivity of photosynthesis in a C_4 plant,
1252 maize, to heat stress. *Plant physiology* **129**, 1773–1780.
1253 Crisp P.A., Ganguly D., Eichten S.R., Borevitz J.O. & Pogson B.J. (2016) Reconsidering
1254 plant memory: Intersections between stress recovery, RNA turnover, and
1255 epigenetics. *Science advances* **2**, e1501340.
1256 Crozet P., Navarro F.J., Willmund F., Mehrshahi P., Bakowski K., Lauersen K.J., …
1257 Lemaire S.D. (2018) Birth of a photosynthetic chassis: A MoClo toolkit enabling
1258 synthetic biology in the microalga *Chlamydomonas reinhardtii*. *ACS synthetic*
1259 *biology* **7**, 2074–2086.
1260 Dhokane D., Bhadra B. & Dasgupta S. (2020) CRISPR based targeted genome editing
1261 of *Chlamydomonas reinhardtii* using programmed Cas9-gRNA ribonucleoprotein.
1262 *Molecular biology reports* **47**, 8747–8755.
1263 van Dongen J.T., Gupta K.J., Ramírez-Aguilar S.J., Araújo W.L., Nunes-Nesi A. & Fernie
1264 A.R. (2011) Regulation of respiration in plants: a role for alternative metabolic
1265 pathways. *Journal of plant physiology* **168**, 1434–1443.
1266 Duncan R.F. & Hershey J.W. (1989) Protein synthesis and protein phosphorylation during
1267 heat stress, recovery, and adaptation. *The Journal of cell biology* **109**, 1467–1481.
1268 Emrich-Mills T.Z., Yates G., Barrett J., Girr P., Grouneva I., Lau C.S., … Mackinder L.C.M.
1269 (2021) A recombineering pipeline to clone large and complex genes in
1270 Chlamydomonas. *The Plant Cell* **33**, 1161–1181.

1271 Fauser F., Vilarrasa-Blasi J., Onishi M., Ramundo S., Patena W., Millican M., … Jinkerson
1272 R.E. (2022) Systematic characterization of gene function in the photosynthetic alga
1273 Chlamydomonas reinhardtii. *Nature genetics* **54**, 705–714.
1274 Friedrich T., Oberkofler V., Trindade I., Altmann S., Brzezinka K., Lämke J., … Bäurle I.
1275 (2021) Heteromeric HSFA2/HSFA3 complexes drive transcriptional memory after
1276 heat stress in Arabidopsis. *Nature communications* **12**, 3426.
1277 Greiner A., Kelterborn S., Evers H., Kreimer G., Sizova I. & Hegemann P. (2017)
1278 Targeting of photoreceptor genes in *Chlamydomonas reinhardtii* via zinc-finger
1279 nucleases and CRISPR/Cas9. *The Plant cell* **29**, 2498–2518.
1280 Grossman-Haham I., Coudray N., Yu Z., Wang F., Zhang N., Bhabha G. & Vale R.D.
1281 (2021) Structure of the radial spoke head and insights into its role in
1282 mechanoregulation of ciliary beating. *Nature structural & molecular biology* **28**, 20–
1283 28.
1284 Guo M., Liu J.-H., Ma X., Luo D.-X., Gong Z.-H. & Lu M.-H. (2016) The Plant Heat Stress
1285 Transcription Factors (HSFs): Structure, Regulation, and Function in Response to
1286 Abiotic Stresses. *Frontiers in plant science* **7**, 114.
1287 Gupta R. & Deswal R. (2012) Low temperature stress modulated secretome analysis and
1288 purification of antifreeze protein from Hippophae rhamnoides, a Himalayan wonder
1289 plant. *Journal of proteome research* **11**, 2684–2696.
1290 Harris E.H. (2009) The Chlamydomonas Sourcebook: Introduction to Chlamydomonas
1291 and Its Laboratory Use: Volume 1. Academic Press.
1292 Hemme D., Veyel D., Mühlhaus T., Sommer F., Jüppner J., Unger A.-K., … Schroda M.
1293 (2014) Systems-wide analysis of acclimation responses to long-term heat stress
1294 and recovery in the photosynthetic model organism *Chlamydomonas reinhardtii*.
1295 *The Plant cell* **26**, 4270–4297.
1296 Hennacy J.H. & Jonikas M.C. (2020) Prospects for engineering biophysical CO_2
1297 concentrating mechanisms into land Plants to enhance yields. *Annual review of*
1298 *plant biology* **71**, 461–485.
1299 Hu B., Jin J., Guo A.-Y., Zhang H., Luo J. & Gao G. (2015) GSDS 2.0: an upgraded gene
1300 feature visualization server. *Bioinformatics* **31**, 1296–1297.
1301 Hu H. & Du J. (2022) Structure and mechanism of histone methylation dynamics in
1302 Arabidopsis. *Current opinion in plant biology* **67**, 102211.
1303 Jagadish S.V.K., Pal M., Sukumaran S., Parani M. & Siddique K.H.M. (2020) Heat stress
1304 resilient crops for future hotter environments. *Plant Physiology Reports* **25**, 529–
1305 532.
1306 Jamloki A., Bhattacharyya M., Nautiyal M.C. & Patni B. (2021) Elucidating the relevance
1307 of high temperature and elevated CO2 in plant secondary metabolites (PSMs)
1308 production. *Heliyon* **7**, e07709.
1309 Janni M., Gullì M., Maestri E., Marmiroli M., Valliyodan B., Nguyen H.T. & Marmiroli N.
1310 (2020) Molecular and genetic bases of heat stress responses in crop plants and
1311 breeding for increased resilience and productivity. *Journal of experimental botany*
1312 **71**, 3780–3802.
1313 Järvi S., Suorsa M. & Aro E.-M. (2015) Photosystem II repair in plant chloroplasts—
1314 regulation, assisting proteins and shared components with photosystem II
1315 biogenesis. *Biochimica et Biophysica Acta (BBA)-Bioenergetics* **1847**, 900–909.

1316 Jin J., Tian F., Yang D.-C., Meng Y.-Q., Kong L., Luo J. & Gao G. (2017) PlantTFDB 4.0:
1317 toward a central hub for transcription factors and regulatory interactions in plants.
1318 *Nucleic acids research* **45**, D1040–D1045.
1319 Johnson X. & Alric J. (2012) Interaction between starch breakdown, acetate assimilation,
1320 and photosynthetic cyclic electron flow in *Chlamydomonas reinhardtii*. *The Journal*
1321 *of biological chemistry* **287**, 26445–26452.
1322 Johnson X. & Alric J. (2013) Central carbon metabolism and electron transport in
1323 *Chlamydomonas reinhardtii*: metabolic constraints for carbon partitioning between
1324 oil and starch. *Eukaryotic cell* **12**, 776–793.
1325 Kamp H.D. & Higgins D.E. (2011) A protein thermometer controls temperature-dependent
1326 transcription of flagellar motility genes in Listeria monocytogenes. *PLoS pathogens*
1327 **7**, e1002153.
1328 Kantidze O.L., Velichko A.K., Luzhin A.V. & Razin S.V. (2016) Heat Stress-Induced DNA
1329 Damage. *Acta naturae* **8**, 75–78.
1330 Karpowicz S.J., Prochnik S.E., Grossman A.R. & Merchant S.S. (2011) The GreenCut2
1331 resource, a phylogenomically derived inventory of proteins specific to the plant
1332 lineage. *The Journal of biological chemistry* **286**, 21427–21439.
1333 Kim S.Y., Slattery R.A. & Ort D.R. (2020) A role for differential Rubisco activase isoform
1334 expression in C_4 bioenergy grasses at high temperature. *GCB Bioenergy* **13**, 211–
1335 223.
1336 Königshofer H., Tromballa H.-W. & Löppert H.-G. (2008) Early events in signaling high-
1337 temperature stress in tobacco BY2 cells involve alterations in membrane fluidity
1338 and enhanced hydrogen peroxide production. *Plant, cell & environment* **31**, 1771–
1339 1780.
1340 Krause C., Richter S., Knöll C. & Jürgens G. (2013) Plant secretome - from cellular
1341 process to biological activity. *Biochimica et biophysica acta* **1834**, 2429–2441.
1342 Kropat J., Hong-Hermesdorf A., Casero D., Ent P., Castruita M., Pellegrini M., …
1343 Malasarn D. (2011) A revised mineral nutrient supplement increases biomass and
1344 growth rate in Chlamydomonas reinhardtii. *The Plant journal: for cell and molecular*
1345 *biology* **66**, 770–780.
1346 Langfelder P. & Horvath S. (2008) WGCNA: an R package for weighted correlation
1347 network analysis. *BMC bioinformatics* **9**, 559.
1348 Larkindale J., Hall J.D., Knight M.R. & Vierling E. (2005) Heat stress phenotypes of
1349 Arabidopsis mutants implicate multiple signaling pathways in the acquisition of
1350 thermotolerance. *Plant physiology* **138**, 882–897.
1351 Lê S., Josse J. & Husson F. (2008) FactoMineR: An R package for multivariate analysis.
1352 *Journal of statistical software* **25**, 1–18.
1353 Li X., Fauser F., Jinkerson R.E., Saroussi S., Meyer M.T., Ivanova N., … Jonikas M.C.
1354 (2019) A genome-wide algal mutant library and functional screen identifies genes
1355 required for eukaryotic photosynthesis. *Nature genetics* **51**, 627–635.
1356 Li X., Zhang R., Patena W., Gang S.S., Blum S.R., Ivanova N., … Jonikas M.C. (2016)
1357 An indexed, mapped mutant library enables reverse genetics studies of biological
1358 processes in *Chlamydomonas reinhardtii*. *The Plant cell* **28**, 367–387.
1359 Mackinder L.C.M. (2018) TheChlamydomonasCO_2-concentrating mechanism and its
1360 potential for engineering photosynthesis in plants. *The New phytologist* **217**, 54–
1361 61.

1362 Martinière A., Shvedunova M., Thomson A.J.W., Evans N.H., Penfield S., Runions J. &
1363 McWatters H.G. (2011) Homeostasis of plasma membrane viscosity in fluctuating
1364 temperatures. *The New phytologist* **192**, 328–337.
1365 McConnell E.W., Werth E.G. & Hicks L.M. (2018) The phosphorylated redox proteome of
1366 Chlamydomonas reinhardtii: Revealing novel means for regulation of protein
1367 structure and function. *Redox biology* **17**, 35–46.
1368 Merchant S.S., Prochnik S.E., Vallon O., Harris E.H., Karpowicz S.J., Witman G.B., …
1369 Grossman A.R. (2007) The *Chlamydomonas* genome reveals the evolution of key
1370 animal and plant functions. *Science* **318**, 245–250.
1371 Minagawa J. & Tokutsu R. (2015) Dynamic regulation of photosynthesis in
1372 *Chlamydomonas reinhardtii*. *The Plant journal: for cell and molecular biology* **82**,
1373 413–428.
1374 Mittler R., Finka A. & Goloubinoff P. (2012) How do plants feel the heat? *Trends in*
1375 *biochemical sciences* **37**, 118–125.
1376 Mueller-Cajar O. (2017) The diverse AAA+ machines that repair inhibited Rubisco active
1377 sites. *Frontiers in Molecular Biosciences* **4**, 31.
1378 Nagarajan R. & Gill K.S. (2018) Evolution of Rubisco activase gene in plants. *Plant*
1379 *molecular biology* **96**, 69–87.
1380 Ngara R., Ramulifho E., Movahedi M., Shargie N.G., Brown A.P. & Chivasa S. (2018)
1381 Identifying differentially expressed proteins in sorghum cell cultures exposed to
1382 osmotic stress. *Scientific reports* **8**, 8671.
1383 Ngcala M.G., Goche T., Brown A.P., Chivasa S. & Ngara R. (2020) Heat Stress Triggers
1384 Differential Protein Accumulation in the Extracellular Matrix of Sorghum Cell
1385 Suspension Cultures. *Proteomes* **8**.
1386 Niemeyer J., Scheuring D., Oestreicher J., Morgan B. & Schroda M. (2021) Real-time
1387 monitoring of subcellular H2O2 distribution in *Chlamydomonas reinhardtii*. *The*
1388 *Plant cell*.
1389 Oberkofler V., Pratx L. & Bäurle I. (2021) Epigenetic regulation of abiotic stress memory:
1390 maintaining the good things while they last. *Current opinion in plant biology* **61**,
1391 102007.
1392 Ortiz-Bobea A., Wang H., Carrillo C.M. & Ault T.R. (2019) Unpacking the climatic drivers
1393 of US agricultural yields. *Environmental research letters: ERL [Web site]* **14**,
1394 064003.
1395 Pandey A., Rajamani U., Verma J., Subba P., Chakraborty N., Datta A., … Chakraborty
1396 N. (2010) Identification of extracellular matrix proteins of rice (Oryza sativa L.)
1397 involved in dehydration-responsive network: a proteomic approach. *Journal of*
1398 *proteome research* **9**, 3443–3464.
1399 Perdomo J.A., Capó-Bauçà S., Carmo-Silva E. & Galmés J. (2017) Rubisco and Rubisco
1400 Activase Play an Important Role in the Biochemical Limitations of Photosynthesis
1401 in Rice, Wheat, and Maize under High Temperature and Water Deficit. *Frontiers in*
1402 *plant science* **8**.
1403 Pérez-Pérez M.E., Mauriès A., Maes A., Tourasse N.J., Hamon M., Lemaire S.D. &
1404 Marchand C.H. (2017) The Deep Thioredoxome in Chlamydomonas reinhardtii:
1405 New Insights into Redox Regulation. *Molecular plant* **10**, 1107–1125.

1406 Picariello T., Hou Y., Kubo T., McNeill N.A., Yanagisawa H.-A., Oda T. & Witman G.B.
1407 (2020) TIM, a targeted insertional mutagenesis method utilizing CRISPR/Cas9 in
1408 *Chlamydomonas reinhardtii*. *PloS one* **15**, e0232594.
1409 Plaxton W.C. (1996) The Organization and Regulation of Plant Glycolysis. *Annual review*
1410 *of plant physiology and plant molecular biology* **47**, 185–214.
1411 Plöchinger M., Schwenkert S., von Sydow L., Schröder W.P. & Meurer J. (2016)
1412 Functional Update of the Auxiliary Proteins PsbW, PsbY, HCF136, PsbN, TerC
1413 and ALB3 in Maintenance and Assembly of PSII. *Frontiers in plant science* **7**.
1414 Pollock S.V., Colombo S.L., Prout D.L., Godfrey A.C. & Moroney J.V. (2003) Rubisco
1415 Activase Is Required for Optimal Photosynthesis in the Green Alga
1416 *Chlamydomonas reinhardtii* in a Low-CO2 Atmosphere. *Plant Physiology* **133**,
1417 1854–1861.
1418 Pospíšil P. (2016) Production of reactive oxygen species by photosystem II as a response
1419 to light and temperature stress. *Frontiers in plant science* **7**, 1950.
1420 Queitsch C., Hong S.W., Vierling E. & Lindquist S. (2000) Heat shock protein 101 plays
1421 a crucial role in thermotolerance in Arabidopsis. *The Plant cell* **12**, 479–492.
1422 Remm M., Storm C.E.V. & Sonnhammer E.L.L. (2001) Automatic clustering of orthologs
1423 and in-paralogs from pairwise species comparisons. *Journal of molecular biology*
1424 **314**, 1041–1052.
1425 Rollins J.A., Habte E., Templer S.E., Colby T., Schmidt J. & von Korff M. (2013) Leaf
1426 proteome alterations in the context of physiological and morphological responses
1427 to drought and heat stress in barley (Hordeum vulgare L.). *Journal of experimental*
1428 *botany* **64**, 3201–3212.
1429 Romero-Campero F.J., Perez-Hurtado I., Lucas-Reina E., Romero J.M. & Valverde F.
1430 (2016) ChlamyNET: a Chlamydomonas gene co-expression network reveals
1431 global properties of the transcriptome and the early setup of key co-expression
1432 patterns in the green lineage. *BMC genomics* **17**, 227.
1433 Rütgers M., Muranaka L.S., Schulz-Raffelt M., Thoms S., Schurig J., Willmund F. &
1434 Schroda M. (2017) Not changes in membrane fluidity but proteotoxic stress
1435 triggers heat shock protein expression in *Chlamydomonas reinhardtii*. *Plant, cell &*
1436 *environment* **40**, 2987–3001.
1437 Rysiak A., Dresler S., Hanaka A., Hawrylak-Nowak B., Strzemski M., Kováčik J., …
1438 Wójciak M. (2021) High Temperature Alters Secondary Metabolites and
1439 Photosynthetic Efficiency in Heracleum sosnowskyi. *International journal of*
1440 *molecular sciences* **22**.
1441 Sage R.F. (2004) The evolution of C_4 photosynthesis. *The New phytologist* **161**, 341–
1442 370.
1443 Saidi Y., Finka A., Muriset M., Bromberg Z., Weiss Y.G., Maathuis F.J.M. & Goloubinoff
1444 P. (2009) The heat shock response in moss plants is regulated by specific calcium-
1445 permeable channels in the plasma membrane. *The Plant cell* **21**, 2829–2843.
1446 Scafaro A.P., Haynes P.A. & Atwell B.J. (1/2010) Physiological and molecular changes
1447 in Oryza meridionalis Ng., a heat-tolerant species of wild rice. *Journal of*
1448 *experimental botany* **61**, 191–202.
1449 Scharf K.D. & Nover L. (1982) Heat-shock-induced alterations of ribosomal protein
1450 phosphorylation in plant cell cultures. *Cell* **30**, 427–437.

1451 Schmollinger S., Strenkert D. & Schroda M. (2010) An inducible artificial microRNA
1452 system for *Chlamydomonas reinhardtii* confirms a key role for heat shock factor 1
1453 in regulating thermotolerance. *Current genetics* **56**, 383–389.
1454 Schroda M., Hemme D. & Mühlhaus T. (2015) The Chlamydomonas heat stress
1455 response. *The Plant journal: for cell and molecular biology* **82**, 466–480.
1456 Schulz-Raffelt M., Lodha M. & Schroda M. (2007) Heat shock factor 1 is a key regulator
1457 of the stress response in *Chlamydomonas*. *The Plant journal: for cell and*
1458 *molecular biology* **52**, 286–295.
1459 Sekiguchi M., Kameda S., Kurosawa S., Yoshida M. & Yoshimura K. (2018) Thermotaxis
1460 in Chlamydomonas is brought about by membrane excitation and controlled by
1461 redox conditions. *Scientific reports* **8**, 16114.
1462 Sengupta P. & Garrity P. (2013) Sensing temperature. *Current biology: CB* **23**, R304-7.
1463 Sessions A., Burke E., Presting G., Aux G., McElver J., Patton D., … Goff S.A. (2002) A
1464 high-throughput Arabidopsis reverse genetics system. *The Plant cell* **14**, 2985–
1465 2994.
1466 Sharkey T.D. (2005) Effects of moderate heat stress on photosynthesis: importance of
1467 thylakoid reactions, rubisco deactivation, reactive oxygen species, and
1468 thermotolerance provided by isoprene. *Plant, cell & environment* **28**, 269–277.
1469 Sharkey T.D. & Zhang R. (2010) High temperature effects on electron and proton circuits
1470 of photosynthesis. *Journal of integrative plant biology* **52**, 712–722.
1471 Shimogawara K., Fujiwara S., Grossman A. & Usuda H. (1998) High-efficiency
1472 transformation of *Chlamydomonas reinhardtii* by electroporation. *Genetics* **148**,
1473 1821–1828.
1474 Shivhare D. & Mueller-Cajar O. (07/2017) In vitro characterization of thermostable CAM
1475 Rubisco activase reveals a Rubisco interacting surface loop. *Plant physiology* **174**,
1476 1505–1516.
1477 Song Y., Zhang C., Ge W., Zhang Y., Burlingame A.L. & Guo Y. (2011) Identification of
1478 NaCl stress-responsive apoplastic proteins in rice shoot stems by 2D-DIGE.
1479 *Journal of proteomics* **74**, 1045–1067.
1480 Su Z., Tang Y., Ritchey L.E., Tack D.C., Zhu M., Bevilacqua P.C. & Assmann S.M. (2018)
1481 Genome-wide RNA structurome reprogramming by acute heat shock globally
1482 regulates mRNA abundance. *Proceedings of the National Academy of Sciences*
1483 *of the United States of America* **115**, 12170–12175.
1484 Tanveer T., Shaheen K., Parveen S., Kazi A.G. & Ahmad P. (2014) Plant secretomics:
1485 identification, isolation, and biological significance under environmental stress.
1486 *Plant signaling & behavior* **9**, e29426.
1487 Theis J. & Schroda M. (2016) Revisiting the photosystem II repair cycle. *Plant signaling*
1488 *& behavior* **11**, e1218587.
1489 Tomsig J.L. & Creutz C.E. (2002) Copines: a ubiquitous family of Ca^{2+}-dependent
1490 phospholipid-binding proteins. *Cellular and molecular life sciences: CMLS* **59**,
1491 1467–1477.
1492 Ueda M. & Seki M. (2020) Histone Modifications Form Epigenetic Regulatory Networks
1493 to Regulate Abiotic Stress Response. *Plant physiology* **182**, 15–26.
1494 Venn B. & Mühlhaus T. (2022) *CSBiology/OntologyEnrichment: Release 0.0.1*.
1495 Venn B., Mühlhaus T., Schneider K., Weil L., Zimmer D., Ziegler S., … venkashank (2022)
1496 *fslaborg/FSharp.Stats: Release 0.4.7*.

1497 Ves-Urai P., Krobthong S., Thongsuk K., Roytrakul S. & Yokthongwattana C. (2021)
1498 Comparative secretome analysis between salinity-tolerant and control
1499 Chlamydomonas reinhardtii strains. *Planta* **253**, 68.
1500 Vu L.D., Gevaert K. & De Smet I. (2019) Feeling the Heat: Searching for Plant
1501 Thermosensors. *Trends in plant science* **24**, 210–219.
1502 Wang D., Li X.-F., Zhou Z.-J., Feng X.-P., Yang W.-J. & Jiang D.-A. (2010) Two Rubisco
1503 activase isoforms may play different roles in photosynthetic heat acclimation in the
1504 rice plant. *Physiologia plantarum* **139**, 55–67.
1505 Wang F., Liu Y., Shi Y., Han D., Wu Y., Ye W., … Yang C. (2020) SUMOylation Stabilizes
1506 the Transcription Factor DREB2A to Improve Plant Thermotolerance. *Plant*
1507 *physiology* **183**, 41–50.
1508 Wang L., Yang L., Wen X., Chen Z., Liang Q., Li J. & Wang W. (2019) Rapid and high
1509 efficiency transformation of *Chlamydomonas reinhardtii* by square-wave
1510 electroporation. *Bioscience reports* **39**, BSR20181210.
1511 Wu H.-C., Luo D.-L., Vignols F. & Jinn T.-L. (2012) Heat shock-induced biphasic Ca2+
1512 signature and OsCaM1-1 nuclear localization mediate downstream signalling in
1513 acquisition of thermotolerance in rice (Oryza sativa L.). *Plant, cell & environment*
1514 **35**, 1543–1557.
1515 Wulfert S., Schilasky S. & Krueger S. (2020) Transcriptional and Biochemical
1516 Characterization of Cytosolic Pyruvate Kinases in Arabidopsis thaliana. *Plants* **9**.
1517 Zhang L., Tian L.-H., Zhao J.-F., Song Y., Zhang C.-J. & Guo Y. (2009) Identification of
1518 an apoplastic protein involved in the initial phase of salt stress response in rice root
1519 by two-dimensional electrophoresis. *Plant physiology* **149**, 916–928.
1520 Zhang N., Mattoon E.M., McHargue W., Venn B., Zimmer D., Pecani K., … Zhang R.
1521 (2022) Systems-wide analysis revealed shared and unique responses to moderate
1522 and acute high temperatures in the green alga Chlamydomonas reinhardtii.
1523 *Communications biology* **5**, 460.
1524 Zhang N., Pazouki L., Nguyen H., Jacobshagen S., Bigge B.M., Xia M., … Zhang R.
1525 (2022) Comparative Phenotyping of Two Commonly Used Chlamydomonas
1526 reinhardtii Background Strains: CC-1690 (21gr) and CC-5325 (The CLiP Mutant
1527 Library Background). *Plants* **11**, 585.
1528 Zhang N. & Portis A.R. Jr (1999) Mechanism of light regulation of Rubisco: a specific role
1529 for the larger Rubisco activase isoform involving reductive activation by
1530 thioredoxin-f. *Proceedings of the National Academy of Sciences of the United*
1531 *States of America* **96**, 9438–9443.
1532 Zhang R., Patena W., Armbruster U., Gang S.S., Blum S.R. & Jonikas M.C. (2014) High-
1533 throughput genotyping of green algal mutants reveals random distribution of
1534 mutagenic insertion sites and endonucleolytic cleavage of transforming DNA. *The*
1535 *Plant cell* **26**, 1398–1409.
1536 Zhang R. & Sharkey T.D. (2009) Photosynthetic electron transport and proton flux under
1537 moderate heat stress. *Photosynthesis research* **100**, 29–43.
1538 Zhao C., Liu B., Piao S., Wang X., Lobell D.B., Huang Y., … Asseng S. (2017)
1539 Temperature increase reduces global yields of major crops in four independent
1540 estimates. *Proceedings of the National Academy of Sciences of the United States*
1541 *of America* **114**, 9326–9331.

1542 Zhou L., Bokhari S.A., Dong C.-J. & Liu J.-Y. (2011) Comparative proteomics analysis of
1543 the root apoplasts of rice seedlings in response to hydrogen peroxide. *PloS one* **6**,
1544 e16723.o

High-throughput Identification of Novel Heat Tolerance Genes via Genome-wide Pooled Mutant Screens in the Model Green Alga *Chlamydomonas reinhardtii*

Erin M. Mattoon[1,2], William McHargue[1,2], Catherine E. Bailey[1], Ningning Zhang[1], Chen Chen[3], James Eckhardt[1,6], Chris G. Daum[4], Matt Zane[4], Christa Pennacchio[4], Jeremy Schmutz[4], Ronan C. O'Malley[4&5], Jianlin Cheng[3], Ru Zhang[1,*]

*Corresponding author: Ru Zhang (rzhang@danforthcenter.org)

[1]Donald Danforth Plant Science Center, St. Louis, Missouri 63132, USA;

[2]Plant and Microbial Biosciences Program, Division of Biology and Biomedical Sciences, Washington University in Saint Louis, St. Louis, Missouri 63130, USA;

[3]Department of Electrical Engineering and Computer Science, University of Missouri, Columbia, Missouri 65211, USA;

[4]U.S. Department of Energy, Joint Genome Institute, Lawrence Berkeley National Laboratory, Berkeley, CA, USA;

[5]Environmental Genomics and Systems Biology, Lawrence Berkeley National Laboratory, Berkeley, CA, USA;

[6]Current address: University of California Riverside, Riverside, California, 92521, USA.

Main figures (8) and supplemental figures (3)

Figure 1

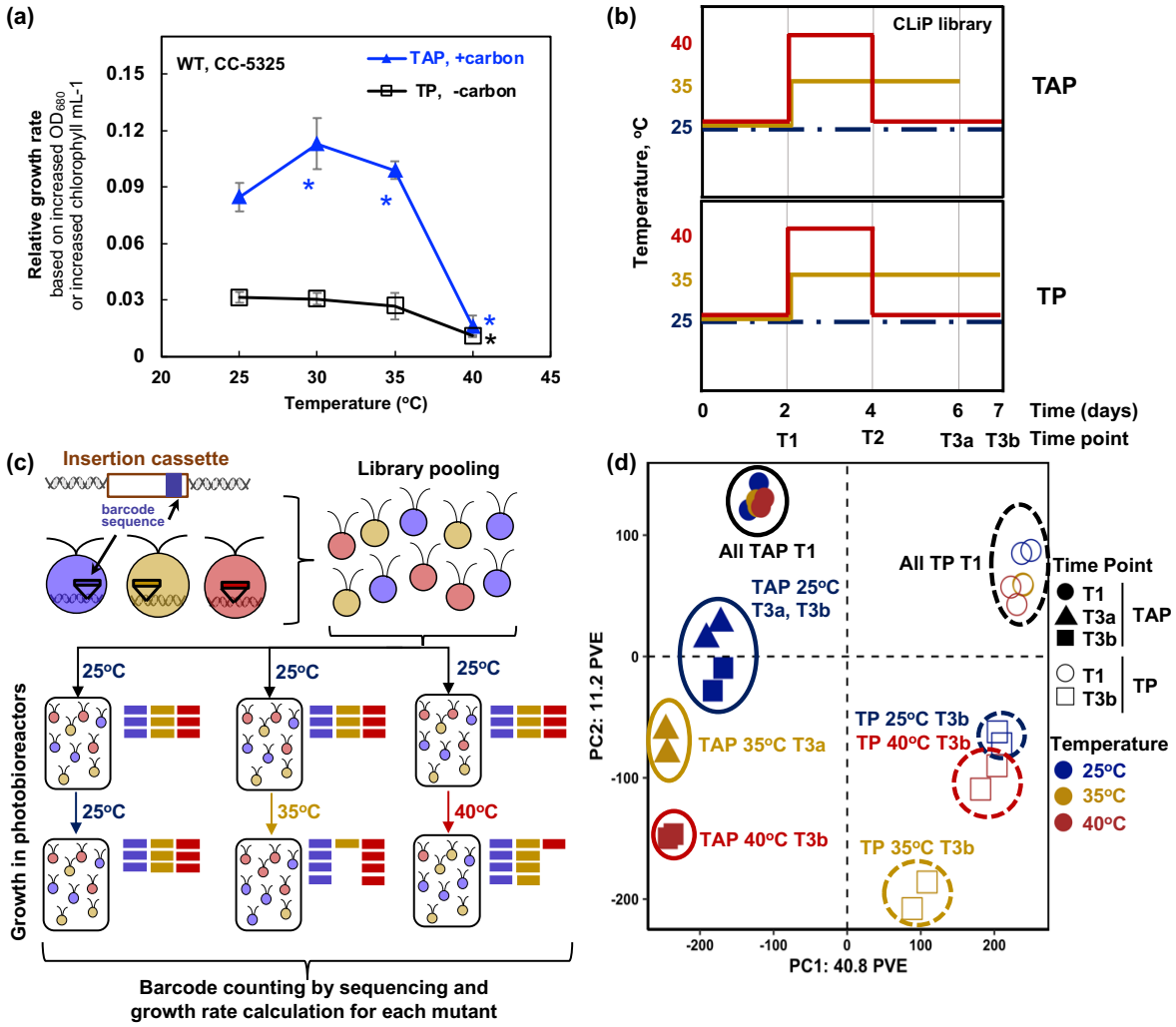

Figure 1: We screened the CLiP Chlamydomonas mutant library under either 35°C or 40°C with and without supplied carbon source using quantitative pooled screens. (a) The relative growth rates of Chlamydomonas wildtype cells (CC-5325, CLiP library background strain) at different temperatures with and without supplied carbon source. Chlamydomonas cells were grown in photobioreactors (PBRs) in Tris-acetate-phosphate (TAP, with acetate, a carbon source) or Tris-phosphate (TP, no acetate) medium under turbidostatic conditions at different temperatures with a light intensity of 100 μmol photons m^{-2} s^{-1} and constantly bubbling of air. Relative growth rates were calculated based on the cycling of OD_{680}, which is proportional to total chlorophyll content in unit of μg chlorophyll mL^{-1}. Each temperature treatment was conducted in an individual PBR and lasted two days. Mean ± SD, n = 2-5 biological replicates. Statistical analyses

were performed using two-tailed t-test assuming unequal variance by comparing with 25°C with the same carbon condition (*, $p < 0.05$, the color and position of asterisks match the treatment conditions). **(b)** Pooled CLiP mutants were grown in PBRs with either TAP or TP medium under different temperature treatments with turbidostatic conditions. Cultures were acclimated for 2 days at 25°C under 100 μmol photons m^{-2} s^{-1} light before high temperature treatments. Heat at 35°C (brown lines) lasted for 4 days (TAP) or 5 days (TP). Heat at 40°C lasted for 2 days then recovered at 25°C for 3 days (red) for both TAP and TP conditions. Algal cultures grown at 40°C for longer than two days could not survive. Control cultures were maintained at 25°C for the duration of the experiment (dark blue). Different treatments were conducted in individual PBRs. Samples were collected at the beginning (T1) and the end (T3a or T3b) of the treatment period. T3a or T3b marked the end of the screens, but T3a was one day shorter than T3b. T3a was used for the end of TAP-35°C screen, while T3b was used for all other screens due to their slower growth rates than TAP-35°C. **(c)** Schematic of pooled screens utilizing unique internal DNA barcodes of the CLiP mutant library. The Chlamydomonas CLiP mutant library enables high-throughput, quantitative phenotyping in pooled cultures. Three hypothetical mutants are shown, each with a unique DNA barcode sequence (represented by purple, brown, and red bars). CLiP mutants are pooled and grown under the condition as in panel b. Under constant 25°C, three mutants have no change of growth rates, thus no change of barcode abundance. If the brown (or red) mutant is deficient in a process essential for optimal growth under a 35°C (or 40°C) screen condition, it will have reduced cell abundance at the end of the screen. Algal cells are harvested at the start and end of the screen for DNA extraction and barcode amplification. Cell abundance and growth rate of each mutant in pooled cultures are calculated by quantifying DNA barcodes using deep sequencing from pooled mutant DNAs. **(d)** Principal component (PC) analysis of normalized barcode abundance from each sample. The first two PC displayed represent the largest amount of variance explained in the dataset. Closed symbols and solid ovals represent TAP conditions, open symbols and dashed ovals represent TP conditions. Colors represent the different temperature treatment groups (blue: 25°C; brown: 35°C; red: 40°C) and shapes represent sampling time points (T1, T3a, T3b). PVE: percent variance explained.

Figure 2

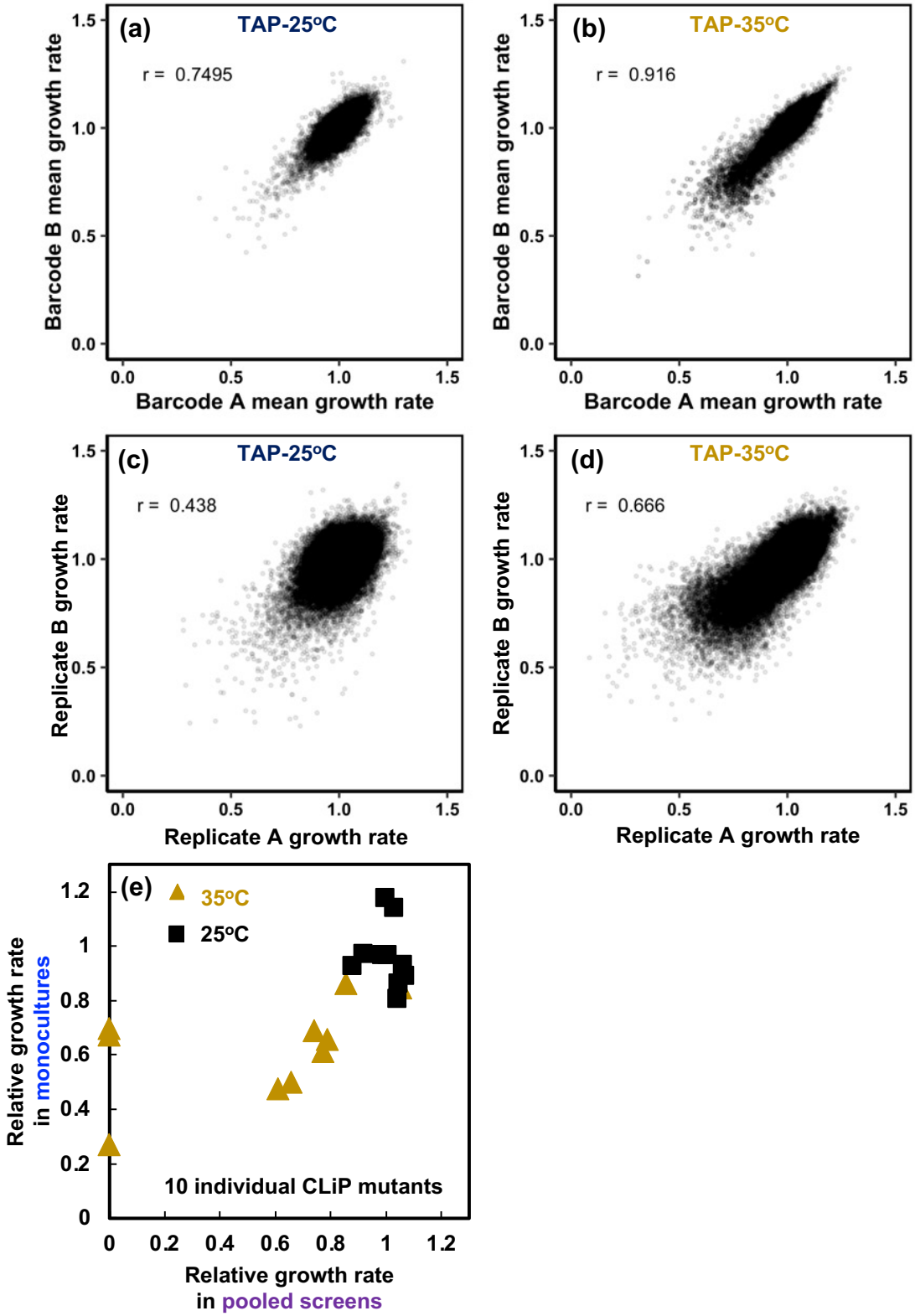

Figure 2: Growth rates calculated from barcode quantification are reproducible. (a, b) Growth rates of one mutant with two different barcodes were consistent. Some mutants

have two different barcodes (from 5' and 3' side of the insertional cassette or from 2 different insertion sites). Different barcodes from the same mutants were amplified and sequenced separately. Each dot represents one mutant with two different barcodes. X- and Y-axes are mean normalized growth rates calculated from two different barcodes of the same mutant in the screens of TAP-25°C (a) and TAP-35°C (b). r: Pearson correlation coefficient. **(c, d)** Growth rates of biological replicates can be calculated consistently. Each dot represents the normalized growth rate of one mutant from two biological replicates in the screens of TAP-25°C (c) and TAP-35°C (d). Because the screen pressure was present under TAP-35°C but not TAP-25°C, the growth rate plots from the two conditions are different. **(e)** Growth rates calculated from pooled mutant screens were validated with those calculated from monocultures for 10 individual CLiP mutants. X: mean relative growth rates of individual CLiP mutants from TAP-25°C (black) or TAP-35°C (brown) calculated from pooled mutant screens. Y: relative growth rates of individual CLiP mutants calculated from monoculture growth experiments normalized to WT CC-5325 under the same condition. The identity of mutants used for monocultures were validated by PCR. For monoculture experiments, individual CLiP mutants were grown in PBRs as mentioned in Figure. 1b, like the pooled screens. Two or three bio-replicates were conducted for most of the CLiP mutants (see mutant IDs and No. of replicates in Supplemental Dataset 1b). Mutants that were depleted in the heat screens were set to have a growth rate of zero in the pooled screens for the plot.

Figure 3

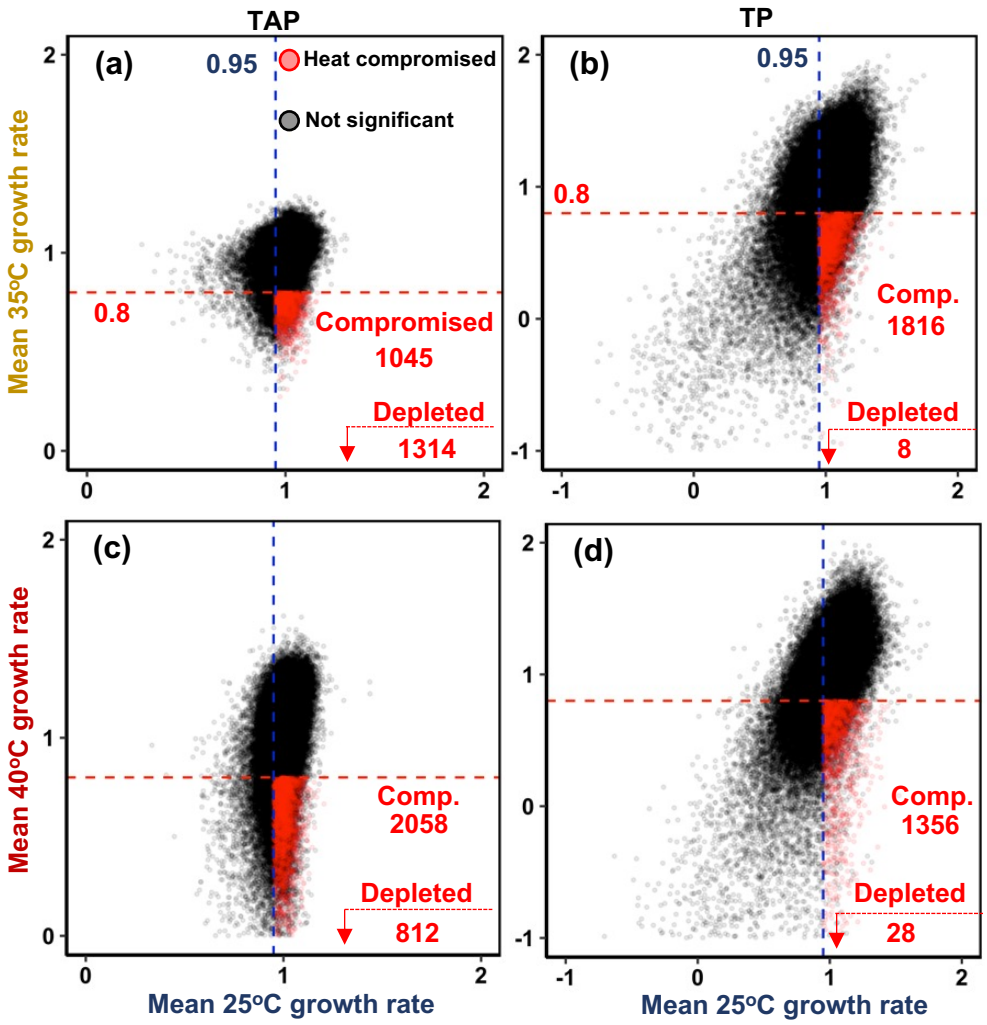

Figure 3: Heat-compromised and heat-depleted mutants were identified from quantitative pooled screens. (a-d) Heat-compromised (comp-) mutants from TAP-35ºC (**a**), TP-35ºC (**b**), TAP-40ºC (**c**), TP-40ºC (**d**) were defined as those with mean normalized growth rates at 25ºC ≥ 0.95, mean normalized growth rates at 35ºC or 40ºC ≤ 0.8, p-value < 0.05 and t-values in the 95th percentile (student's one-sided t-test of unequal variance, red dots). Heat-depleted individuals were defined as those that were absent from the 35ºC or 40ºC pools at the end of the screen but had normal growth at 25ºC (≥0.95), indicated in the bottom right corner of each panel.

Figure 4

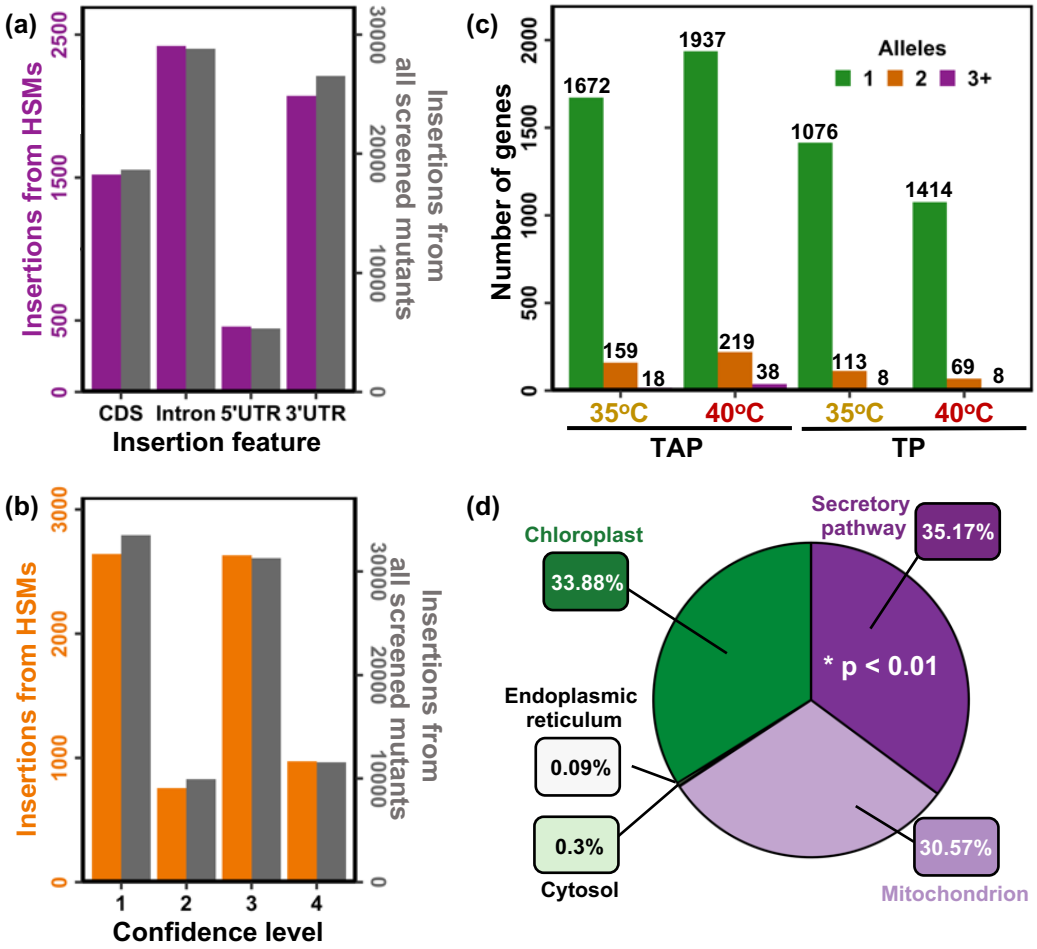

Figure 4: Heat sensitive mutants disrupted in putative heat tolerance genes (HTGs) were characterized at the genome-wide level. Each CLiP mutant has a mapped insertion site, thus a mapped disrupted gene. We identified putative HTGs from heat sensitive mutants (HSMs). **(a)** Distribution of insertion features from HSMs (purple) is similar to that from the CLiP library screened (gray). Insertion feature refers to the integration sites of the transforming cassette relative to gene components, e.g., untranslated regions (UTRs), coding sequence (CDS), or introns. **(b)** Distribution of confidence levels from HSMs (orange) is similar to that from the CLiP library screened (gray). Insertion confidence refers the likelihood of the mapped insertion sites being correctly identified based on genomic sequences flanking the insertional cassette, with levels 1 and 2 for the highest confidence (95%) of the mapped insertion sites, level 3 for 73% confidence, level 4 for 58% confidence. **(c)** For HTGs identified from each of the four

treatment conditions, the number of alleles that were significantly heat sensitive are shown. Green, orange, and purple bars represent 1, 2, or ≥ 3 heat sensitive alleles, respectively. **(d)** HTGs identified in any of the four treatment conditions were aggregated and the distribution of predicted subcellular localizations is displayed. Significant enrichment for the secretory pathway was found (*, Fisher's exact test, $p < 0.01$). Percentage shown of each localization is the % of HTGs with this predicted subcellular localization out of all HTGs identified with a predicted subcellular localization.

Figure 5

(a)

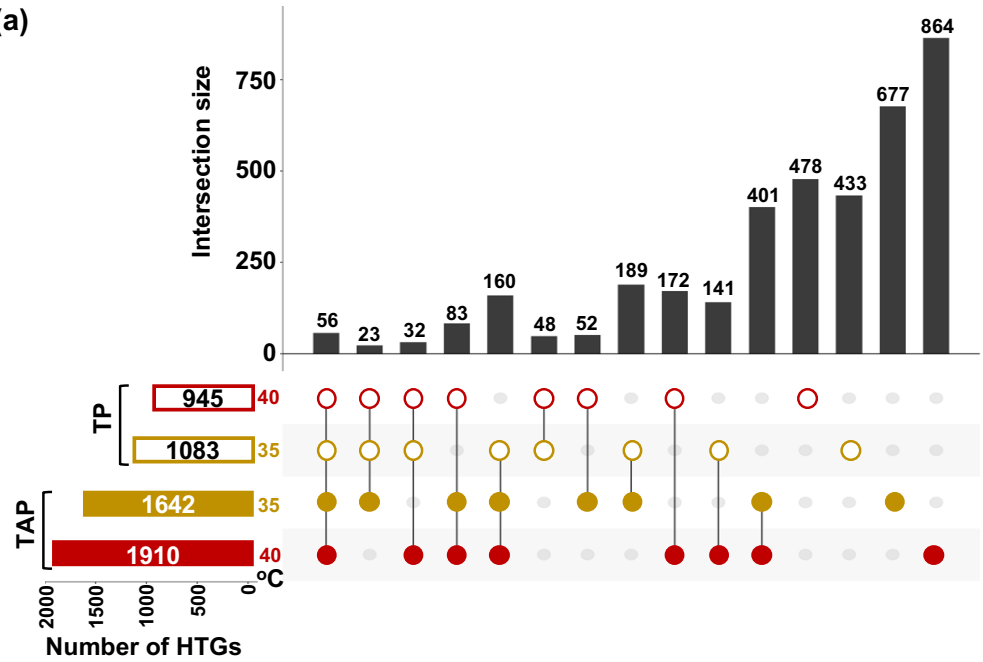
Intersection size
750
500
250
0
56
23
32
83
160
48
52
189
172
141
401
478
433
677
864
TP
945
40
1083
35
TAP
1642
35
1910
40
°C
2000
1500
1000
500
0
Number of HTGs

(b)

transport.calcium (26)
signalling.unspecified (23)
signalling.receptor kinases.leucine rich repeat VII (4)
signalling.in sugar and nutrient physiology.misc (34)
signalling.calcium (62)
RNA.regulation of transcription.pseudo ARR transcription factor family (5)
RNA.regulation of transcription.chromatin remodeling factors (42)
PS.lightreaction.hydrogenase.FeFe-hydrogenase (5)
protein.synthesis.ribosomal protein.prokaryotic.chloroplast.30S subunit.S30A (2)
protein.degradation.ubiquitin.E2 (22)
protein.degradation.cysteine protease (35)
protein.aa activation.methionine-tRNA ligase (4)
nucleotide metabolism.synthesis.purine (82)
misc.calcineurin-like phosphoesterase family protein (3)
minor CHO metabolism.sugar alcohols (99)
minor CHO metabolism.callose (49)
lipid metabolism.FA synthesis and FA elongation.pyruvate kinase (3)
glycolysis.unclear/dually targeted.pyruvate kinase (PK) (3)
glycolysis.plastid branch.pyruvate kinase (PK) (2)
glycolysis.cytosolic branch.pyruvate kinase (PK) (5)
fermentation (4)
Co-factor and vitamine metabolism.lipoic acid (4)
cell.organisation.cytoskeleton.actin.Actin (2)
cell.motility.eukaryotes.radial spoke.head (4)
cell.motility.eukaryotes.other (38)
cell.motility.eukaryotes.intraflagellar transport.IFT particle protein.complex B (11)
cell.motility.eukaryotes.intraflagellar transport.IFT motor protein.kinesin-2 subunits (3)
cell.motility.eukaryotes.flagellar associated proteins (100)
cell.motility.eukaryotes.basal bodies (31)
cell.motility.eukaryotes.axonemal dyneins.inner arm.monomeric species (20)
MapMan Term
p.adjust
0.04
0.03
0.02
0.01
No. of genes
10
20
All HTGs
Both TAP
Both TP
Both 35°C
Both 40°C
All Overlap

Figure 5: Heat tolerance genes (HTGs) were overlapped between conditions for functional enrichment. (a) HTGs overlap between conditions. From the identified heat sensitive mutants, we generated a list of genes with potential roles in heat tolerance, defined as HTGs, which are those with at least 1 heat-compromised or heat-depleted mutant in a screen condition under high temperatures. To compare between conditions, only genes represented by at least one mutant in all four conditions were included in this analysis. Horizontal bars represent the total number of HTGs from each condition. Vertical bars and the number on their top represent the number of genes included in each overlap. Circles along x-axis represent the conditions included in each overlap in the vertical bars. Filled circles represent TAP conditions and open circles represent TP conditions; circle colors represent the temperature of heat treatments, brown for 35°C and red for 40°C. Genes belong to only a single intersection category and are sorted into the category with the greatest number of intersections. (**b**) MapMan functional enrichment of all HTGs identified (those with at least one heat sensitive mutant in at least one condition), both TAP conditions, both TP conditions, both 35°C conditions, both 40°C conditions, and all 4 conditions are shown. Only significantly enriched MapMan terms are shown (FDR < 0.05). Size of each circle indicates the number of HTGs in a given MapMan term. Color of the circles represent the FDR adjusted p-value. Numbers in parentheses after each Mapman term is the total number of genes assigned to the given MapMan term and present in the pooled screen dataset.

Figure 6

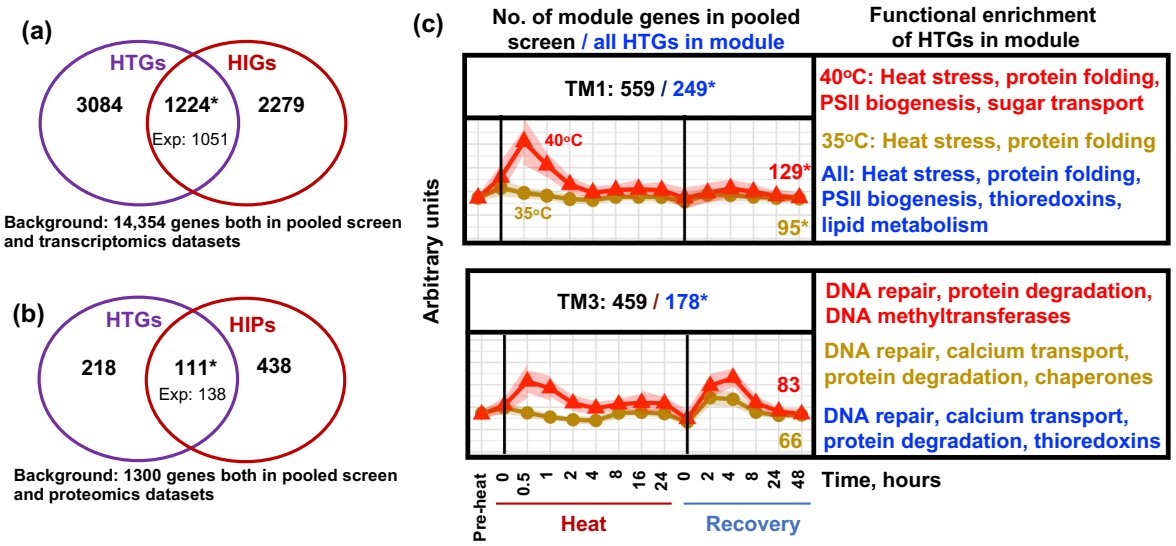

Figure 6: Comparison of heat tolerance genes (HTGs) with transcriptome and proteome data under high temperature. (a, b) Venn diagrams comparing HTGs with heat induced genes/proteins (HIGs/HIPs) from 35°C and 40°C treatments of WT cultures in TAP medium (Zhang *et al.* 2022). Exp, expected overlapping numbers based on random chance. *, $p < 0.05$, Fisher's Exact Test based on the indicated background size. **(c)** Select weighted correlation network analysis (WGCNA) modules that were overrepresented for HTGs above random chance (*, $p < 0.05$, Fisher's exact test). TM: transcriptomic module. Consensus transcription patterns from TAP-40°C (red) and TAP-35°C (brown) are shown. Numbers at the top of each module display: the total number (No.) of genes in the given module that were represented by at least one mutant in the pooled screens (before /, black) and the total No. of aggregated HTGs in that module from all four treatment conditions (after /, blue). Numbers at the right of each plot show the No. of HTGs from TAP-40°C (red, top) and TAP-35°C (brown, bottom), respectively. Functional enrichment on right side of each module shows select significantly enriched MapMan terms from TAP-40°C HTGs (top, red), TAP-35°C HTGs (middle, brown) and the aggregated list of HTGs from all four conditions (bottom, blue) that are present in a given module (FDR < 0.05).

Figure 7

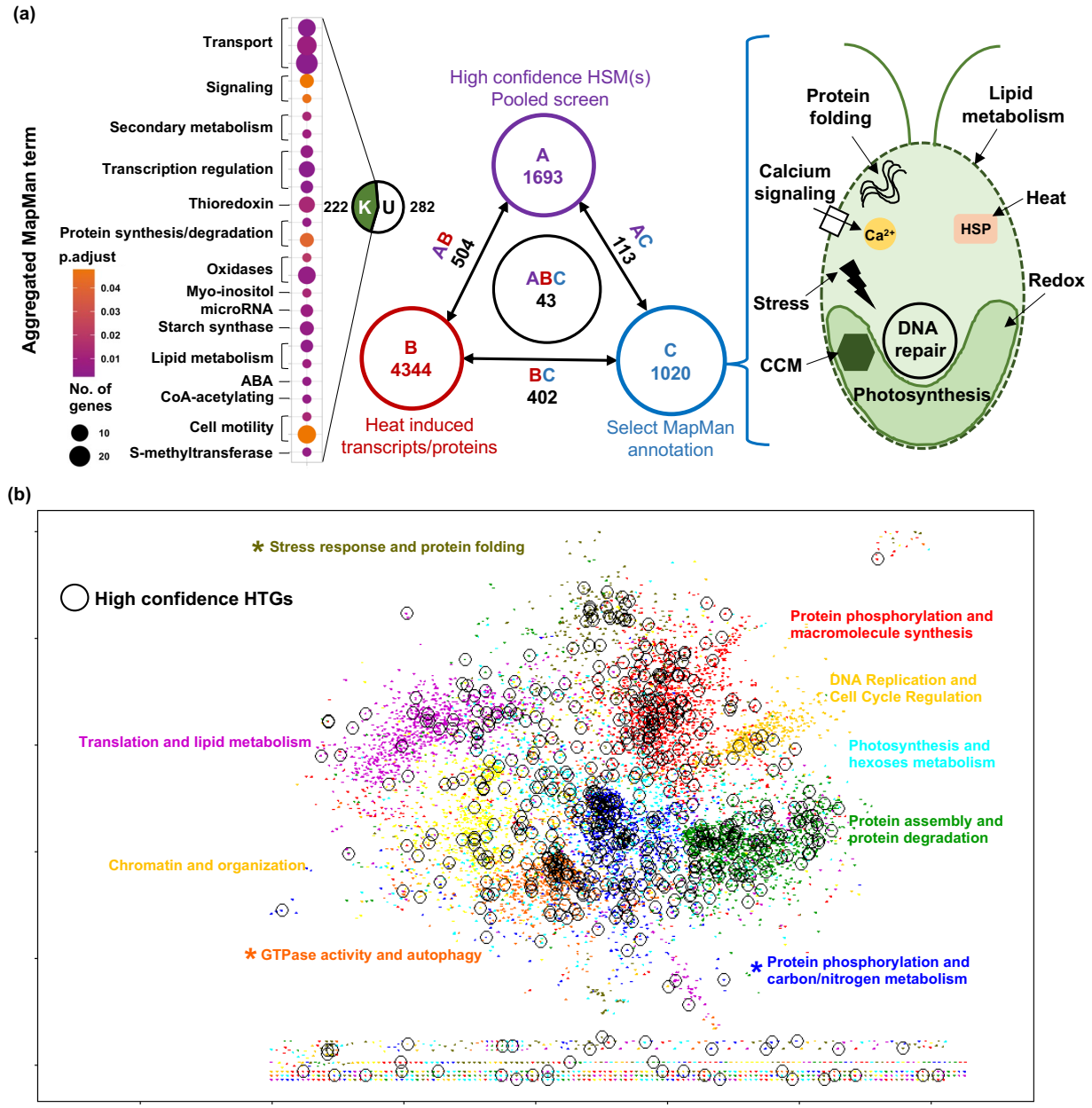

Figure 7: A triangulation approach was used to identify high confidence heat tolerance genes (HTGs). (**a**) High confidence HTGs were defined using a triangulation approach based on three criteria: (A): HTGs in our pooled screens that had at least one heat sensitive mutant (HSMs) in at least two conditions or at least two heat sensitive mutant alleles in any one condition (defined as high confidence HSMs); (B): heat inducible during the high temperature treatment of previously published RNA-seq or proteomic

data; (C): MapMan functional annotation in select categories that may be involved in thermotolerance or affected by high temperatures. MapMan functional categories included in this analysis are displayed in cartoon on the right. Genes that meet at least two of these three criteria were considered as high confidence HTGs. The number of genes overlapping between any two categories are displayed next to arrows connecting criteria. Of the 504 genes overlapping between criteria A and B, 282 had no MapMan functional annotations (U) and 222 had at least one MapMan functional annotation (K). Of the 222 genes with functional annotations, functional enrichment analysis with abbreviated MapMan terms is displayed (right). Size of each circle indicates the number of overlapping HTGs in a given MapMan term. Color of the circles represent the adjusted p-value. For full list of MapMan annotations included in this analysis see supplemental dataset 3j. (**b**) Visualization of high confidence HTGs in the transcription network topology of ChlamyNET, a web-based network tool that was generated based on published transcriptomes in Chlamydomonas (Romero-Campero *et al.* 2016). Nine gene clusters with different function enrichment were identified by ChlamyNET, represented by different colors. Each dot represents one Chlamydomonas gene in the network. The genes circled in black are the high confidence HTGs. Of the 933 high confidence HTGs, 594 were present in the ChlamyNET network of 9,171 genes. Stars (*) indicate significant enrichment for high confidence HTGs within the three ChlamyNet clusters (FDR < 0.05). The overrepresentation analysis and scatterplot visualization are performed using the R programming language.

Figure 8

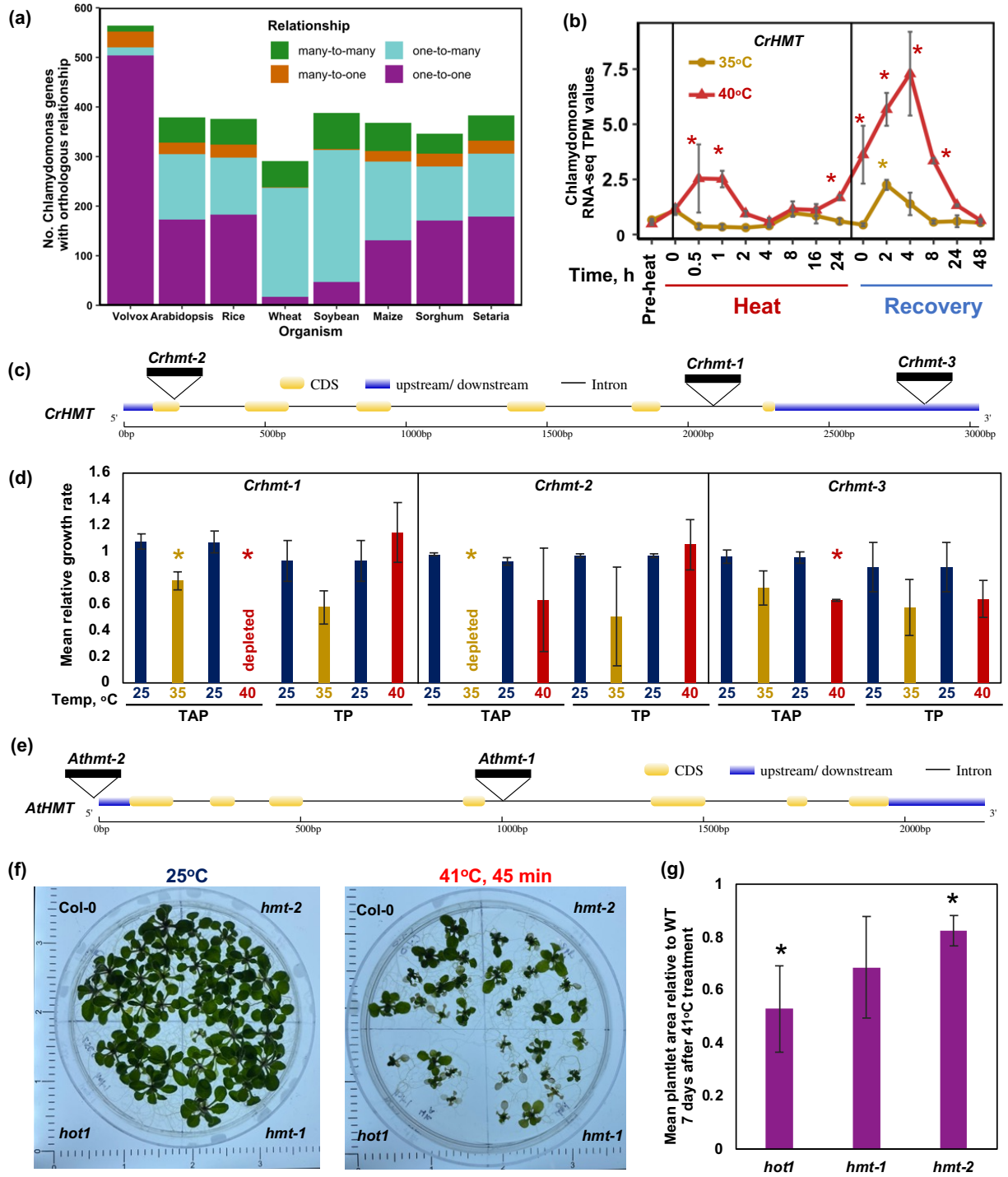

Figure 8: Many Chlamydomonas high confidence heat tolerance genes (HTGs) are conserved throughout the green lineage. (a) Chlamydomonas high confidence HTGs were classified by their orthology to *Volvox carterii* (Volvox), *Arabidopsis thaliana*

(Arabidopsis), *Oryza sativa* (Rice), *Triticum aestivum* (wheat), *Glycine max* (Soybean), *Zea mays* (Maize), *Sorghum bicolor* (Sorghum), and *Setaria viridis* (Setaria) genes using the InParanoid ortholog dataset. **(b)** Mean transcript per million (TPM) normalized read counts of the Chlamydomonas putative histone-lysine N-methyltransferase (HMT) gene during and after high temperatures of 35ºC (brown curve) or 40ºC (red curve) (modified from Zhang et. al., 2022). Mean ± SD, *n*=3. Stars indicate significance in differential expression modeling. (**c, d**) Three CLiP alleles of *CrHMT* were heat sensitive in our pooled mutant screens. Stars indicate significance in pooled screen data. Mean ± SD, *n*=2. (e) Two mutant alleles of Arabidopsis AtHMT (one-to-one ortholog), *Athmt-1* and *Athmt-2* were used for phenotype verification in land plants. (**f**) Representative plate images of 14-day old seedlings from control (25ºC) and treatment (41ºC for 45 minutes followed by 7 days of recovery at 25ºC). (**g**) Mean plantlet area relative to wild type (Col-0) of *hmt-1*, *hmt*-2, and *hot1* (positive control, a well-characterized heat sensitive mutant, deficient in Heat Shock Protein HSP101). Plantlet area was quantified using ImageJ and normalized to the total area of Col-0 on the same plate. Mean ± SD, *n*=3. *, $p < 0.05$, student's one-sided t-test of unequal variance.

Supplemental figures

Figure S1

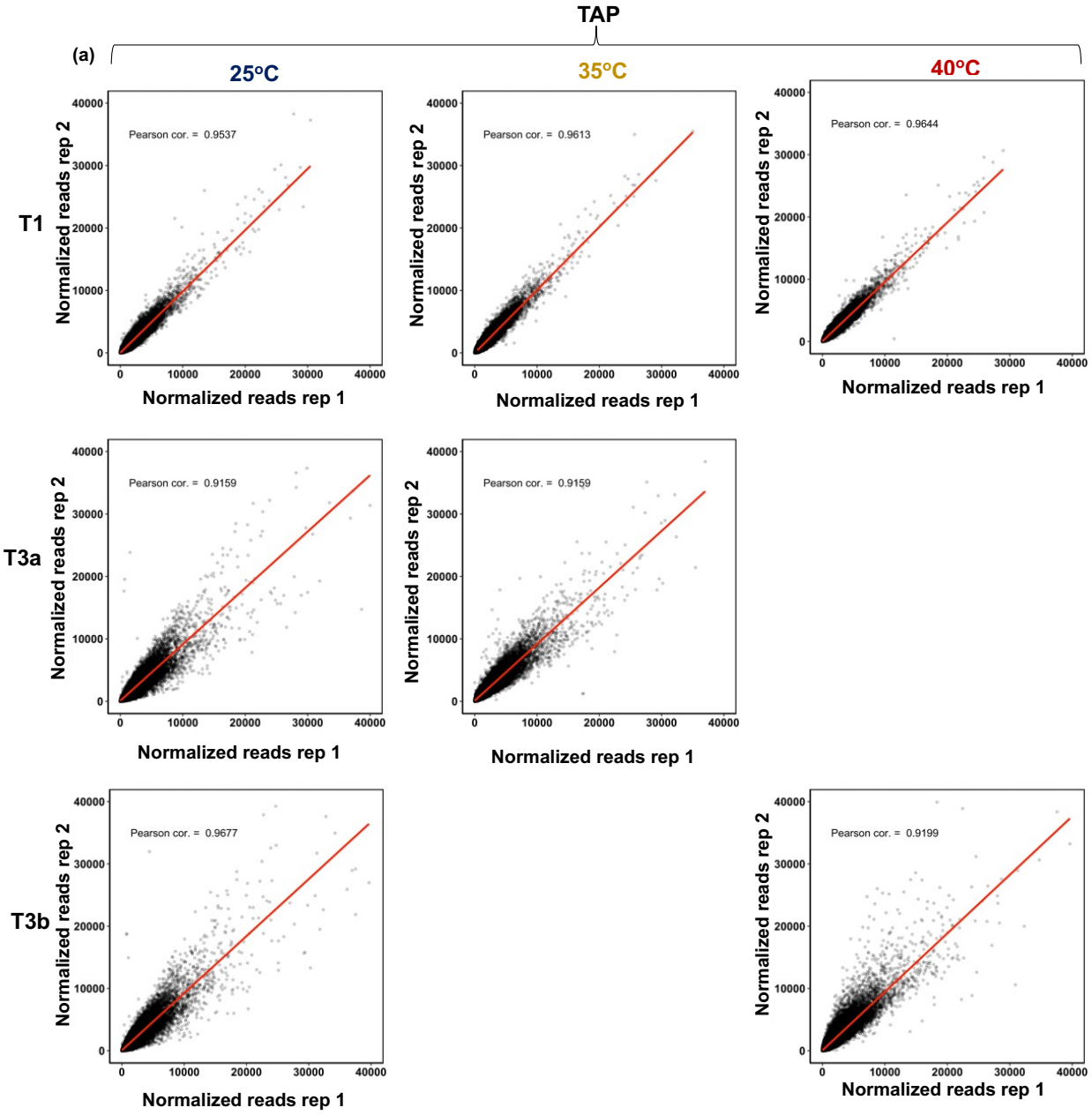

Figure S1

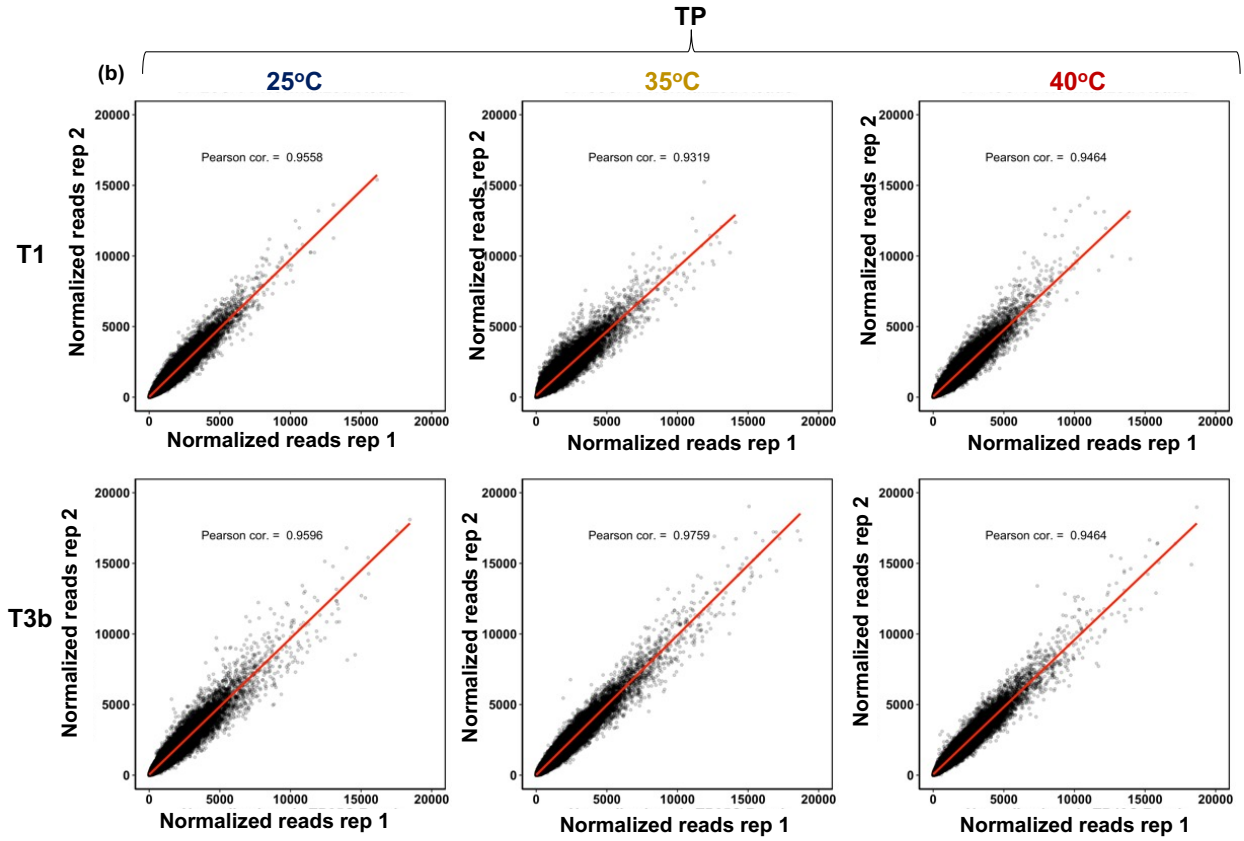

Figure S1: Normalized read counts of biological replicates are highly reproducible. Normalized reads for each barcode in two biological replicates are shown for every condition and time point. Linear model of best fit shown in red line. Pearson correlation coefficient are displayed. Treatment groups are displayed in columns (25ºC, 35ºC, and 40ºC from left to right). Time points are displayed in rows (T1, T3a, T3b from top to bottom. **(a)** All TAP (Tris-acetate-phosphate medium) conditions with supplied carbon source. **(b)** All TP (Tris-phosphate medium) conditions without supplied carbon source.

Figure S2

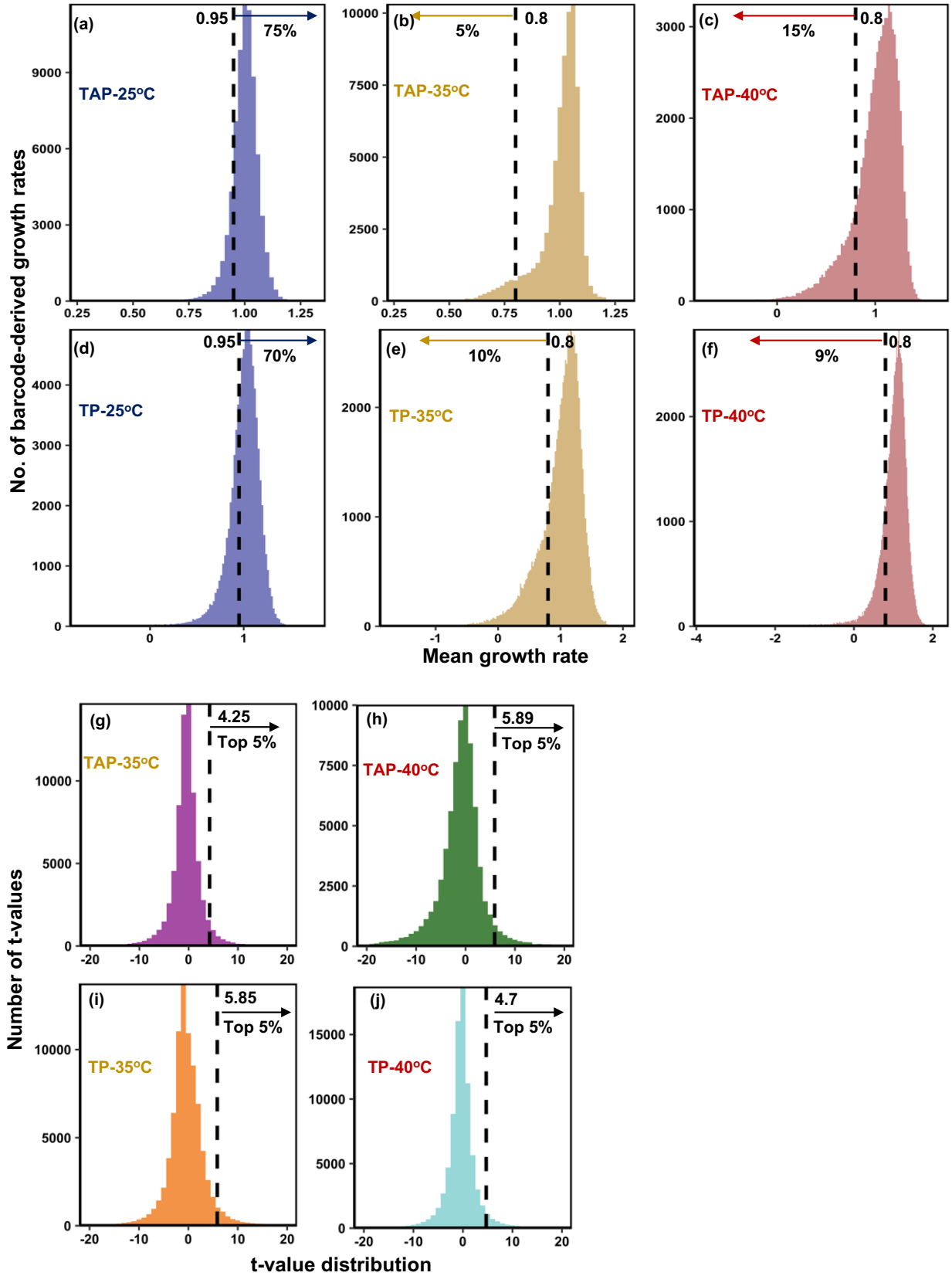
(a)
0.95
75%
TAP-25°C
(b)
0.8
5%
TAP-35°C
(c)
0.8
15%
TAP-40°C
(d)
0.95
70%
TP-25°C
(e)
0.8
10%
TP-35°C
(f)
0.8
9%
TP-40°C
No. of barcode-derived growth rates
Mean growth rate
(g)
4.25
Top 5%
TAP-35°C
(h)
5.89
Top 5%
TAP-40°C
(i)
5.85
Top 5%
TP-35°C
(j)
4.7
Top 5%
TP-40°C
Number of t-values
t-value distribution

Figure S2: We used statistical cutoffs to identify heat sensitive mutants. Heat sensitive mutants are required to have normal growth rates at 25°C (≥ 0.95) and reduced mean normalized growth rates at 35°C or 40°C (≤ 0.8), p-value < 0.05, and t-values in the 95th percentile (student's one-sided t-test of unequal variance). **(a-f)** Distribution of mean growth rates of all mutants in each condition. Dashed lines represent growth rates cutoffs. Growth rate cutoff values are displayed at the start of the arrows. Percentage under the arrows quantifies the fraction of barcodes that meet the growth rate cutoffs. **(g-j)** Empirical distributions of t-values for all tests per condition. T-values are based on both the difference between means and the variance between biological replicates. Vertical dashed lines display the 95th percentile mark for each empirical distribution. Numbers above the arrows display the cutoff t-values. Only the top 5% of t-values were considered statistically significant, in addition to p-values < 0.05.

Figure S3

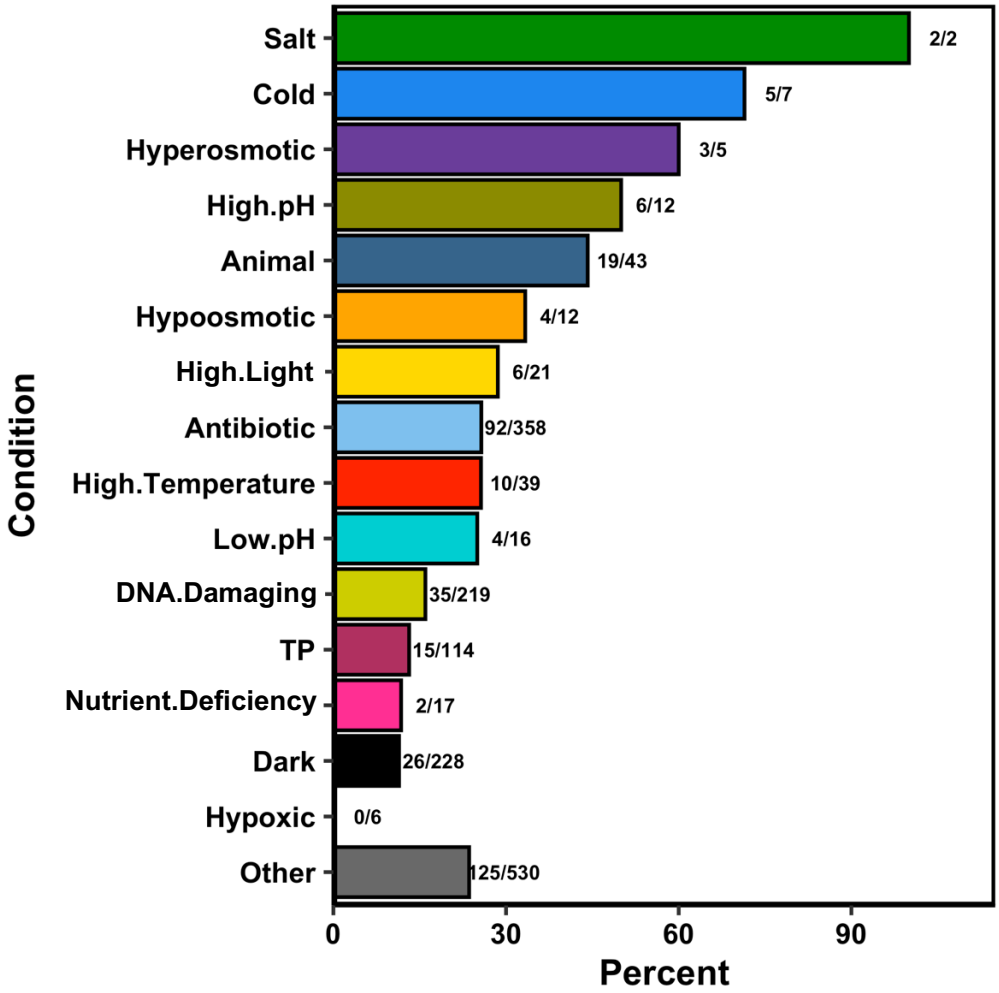

Figure S3: Some heat tolerance genes (HTGs) may be also involved in other stresses. The 1,693 heat tolerance genes (HTGs) with high confidence heat sensitive mutants (HSMs) identified in our screens were compared with previously published screen data (Fauser et al. 2022) from approximately 121 pooled screen conditions, sorted into 16 broad categories with FDR<0.3. These 1693 HTGs refer to those that have at least one HSM in at least two conditions or at least two HSM alleles in any one condition in our pooled screens. Bars quantify the % of overlapping HTGs with sensitive mutants in the given condition (numerator) out of all genes with sensitive mutants in that condition (denominator). Numbers after horizontal bars are No. of genes with significantly sensitive mutants in that condition and also overlap with our HTGs (before /) and No. of genes with significantly sensitive mutants in that condition (after /). The ratios of these two numbers are the % presented by the X axis.